UNIVERSITAT POLITÈCNICA DE CATALUNYA
BARCELONATECH
Escola Superior d'Enginyeries Industrial,
Aeroespacial i Audiovisual de Terrassa

Hydrofoils design for a Europe dinghy

BACHELOR FINAL THESIS

Document:
Report

Author:
Santiago Mañé Ubalde

Director:
José-Antonio Ortiz Marzo

Degree:
Bachelor's degree in Aerospace Vehicle Engineering

Examination session:
Spring, 2021

DECLARATION OF HONOR

I declare that,

- The work in this Bachelor Thesis is completely my work,
- No part of this Bachelor Thesis is taken from other people's work without giving them credit,
- All the references have been cited,
- I am authorised to make use of the data sources from open sources I am providing in this document.

I understand that an infringement of this declaration leaves me subject to the foreseen disciplinary actions by the Universitat Politècnica de Catalunya.

Santiago Mañé Ubalde		**June 22, 2021**
Student Name	*Signature*	*Date*

Title of the Thesis: **Hydrofoils design for a Europe dinghy**

ABSTRACT

This bachelor final thesis contains the development of a hydrofoil kit to be installed in an International Europe Class dinghy. It includes an aerodynamics and hydrodynamics theoretical introduction, as well as a general overview of hydrofoil technology. The thesis follows with the sizing of foiling surfaces through a mathematical study based on the appropriate aerodynamics concepts. The results are validated using the XFLR5 software. Then, the modelling process of the system and control mechanism is shown. Finally, a prototype of the concept is manufactured to demonstrate the viability of the project. The author of this thesis intends to enhance the performance of the International Europe Class dinghy and raise it to the level of foiling dinghies available in the market.

Esta tesis de fin de grado contiene el desarrollo de un "kit" hidroala para ser instalado en una embarcación de vela ligera de la clase Europa. El proyecto incluye una breve introducción de carácter teórico a los campos de la hidrodinámica y aerodinámica, así como al funcionamiento de las hidroalas. Seguidamente, se presenta el proceso de dimensionamiento de las superficies sustentadoras, basado en un estudio matemático que incorpora conceptos relacionados con la aerodinámica. Los resultados obtenidos son validados con el software XFLR5. A continuación, se muestra el proceso de modelado del sistema así como del mecanismo de control que incluye. Finalmente, un prototipo del concepto es fabricado para demostrar la viabilidad del proyecto. El autor de este trabajo quiere mejorar las prestaciones del Europa para que este pueda igualar en rendimiento a los barcos de vela ligera de nueva generación disponibles en el mercado.

Aquesta tesi de fi de grau conté el desenvolupament d'un "kit" hidroala per a ser instal·lat en una embarcació de vela lleugera de la classe Europa. El projecte inclou una breu descripció de caràcter teòric als camps de la hidrodinàmica i aerodinàmica, així com al funcionament de les hidroales. Seguidament, es presenta el procés de dimensionament de les superfícies de sustentació, basat en un estudi matemàtic que incorpora conceptes basats en l'aerodinàmica. Els resultats obtinguts són validats amb el software XFLR5. A continuació es mostra el procés de modelatge del sistema així com del mecanisme de control que incorpora. Finalment, un prototip del concepte és fabricat per demostrar la viabilitat del projecte. L'autor d'aquest treball vol millorar les prestacions de l'Europa perquè aquest pugui igualar en rendiment a les embarcacions de vela lleugera de nova generació disponibles en el mercat.

ACKNOWLEDGMENT

Throughout the writing of this thesis, I have received a great deal of support and assistance. Firstly I would like to thank my supervisor and tutor, Jose-Antonio Ortiz-Marzo, for his interest in this project. Since the day I presented the idea he offered constant support and feedback was crucial for the development of the thesis.

The expertise of Toni Riera from N1Foils was crucial for the manufacturing phase. I would like to thank him and his team for sharing their knowledge about composite manufacturing and contributing to the prototype build. As important was the involvement of my friend and computer science engineer, Andreu Pla, and his 3D printer. Andreu printed all of the moulds and innumerable failed test models. I thank him for his advice, enthusiasm and patience, which shaped many of my ideas for this project into reality. I also have to acknowledge the contribution of classmates and friends Xavier Soria and Marc Martí. Thank you both for your unconditional support through all the career and project.

In addition, I would like to thank all my friends that got involved with this project and my parents and little brother Àlvar for giving advice and being there when I needed it.

TABLE OF CONTENTS

LIST OF TABLES

LIST OF FIGURES

LIST OF SYMBOLS

$C_{m1/4}$	2D moment coefficient at aerodynamic centre
$C_{m1/4}$	2D moment coefficient at aerodynamic centre
$C_{l_{cd,min}}$	2D lift coefficient for minimum drag
$\bar{c}$	Average aerodynamic chord
$C_{d,min}$	Minimum 2D drag coefficient
C_d	2D drag coefficient
C_D	3D drag coefficient
C_{d0}	2D parasite drag coefficient
C_{Di}	3D induced drag coefficient
$C_{l,max}$	Maximum 2D lift coefficient
C_l	2D lift coefficient
C_L	3D lift coefficient
$C_{l\alpha}$	2D lift coefficient slope
$C_{L\alpha}$	3D lift coefficient slope
$C_{l\alpha 0}$	2D lift coefficient y-intercept
$C_{M,cm}$	3D moment coefficient at centre of mass
$C_{M\delta_e}$	3D flap deflection moment coefficient
C_{M0}	3D independent moment coefficient
$C_{M1/4}$	3D moment coefficient at aerodynamic centre
$C_{M\alpha}$	3D moment coefficient slope
c_r	Root chord
c_t	Tip chord
D_i	Induced drag
F_s	Submergence factor
F_x	x-axis force
F_y	y-axis force
h_s	y-axis sailor's position
h_w	z-axis sail pressure centre position
L_1	Centreboard hydrofoil lift
L_2	Rudder hydrofoil lift
m_0	independent wing moment

M_1	Centreboard hydrofoil moment
M_2	Rudder hydrofoil moment
M_w	Wind generated moment
m_α	Dependent wing moment
p_f	y-axis intersection point between 2D and 3D plots (with flap)
S_c	Centreboard foil surface
S_r	Rudder foil surface
u_∞	Free stream speed
w_{bl}	Rudder blade weight
w_{bo}	Boom weight
w_c	Centreboard weight
w_h	Hull weight
w_m	Mast weight
w_s	Sailor weight
w_{st}	Rudder stock weight
w_t	Total weight
X_1	Centreboard foil aerodynamic centre position
X_2	Rudder foil aerodynamic centre position
x_{bl}	Rudder blade centre of mass position
x_{bo}	Boom centre of mass position
x_c	Centreboard centre of mass position
x_h	Hull centre of mass position
x_m	Mast centre of mass position
x_s	Sailor centre of mass position
x_{st}	Rudder stock centre of mass position
α_0	Null lift angle of attack
α_i	Induced angle of attack
α_s	Maximum lift angle of attack
α_w	Wind angle of incidence to the sail
δ_e	Flap deflection
θ_g	Geometrical twist
b	Wind/foil span
c	Aerodynamic chord
D	Drag
e	Oswald efficiency number

F	Force
FoS	Factor of safety
h	Depth of operation
L	Lift
M	Moment
Ma	Mach number
p	y-axis intersection point between 2D and 3D plots
P	Pressure
Re	Reynolds number
S	Surface
Λ	Aspect ratio
W	Wind speed
Xcm_s	Centre of mass with sailor
Xcm	Centre of mass without sailor
α	Angle of attack
δ	Dihedral angle
μ	Dynamic viscosity
π	Pi number
ρ	Density
φ	Swept angle

2. INTRODUCTION

2.1. Aim

This project aims to transform a conventional International Europe Class dinghy into a foiling dinghy, hence reducing the drag produced by the hull allowing it to achieve higher speeds. This conversion implies the design of foiling surfaces as well as the study of the corresponding control mechanism. The result must respect the integrity of the hull while being removable and allow for foiling conditions and medium wind speeds. Moreover, a materials and manufacturing study of the prototype will be carried out to ensure that the construction of it is possible.

2.2. Scope

The Project will include the following areas of development:

- Theoretical introduction to the International Europe Class and hydrodynamics.
- Background study of hydrofoils in dinghy sailing and state of the art review.
- Study of the Europe dinghy performance under a variety of wind conditions.
- Selection of the platform type considering the advantages and disadvantages of each option to meet the requirements.
- Calculations of the foiling surface dimensions and geometry through a mathematical model and theoretical background.
- Testing of the obtained geometries using XLFR5 software.
- Sizing of the control surfaces and selection of a control mechanism.
- CAD design of the foiling device and control mechanism.
- Material selection and manufacturing study.
- Economic feasibility of the project.

2.3. Requirements

Certain requirements must be achieved to consider the project successful. These requisites will be listed below and ensure the viability of the project.

- The converted Europe dinghy must be able to sustain stable hydrofoil sailing under certain wing conditions. This means that the hull must be completely above the water line and maintain a constant altitude without oscillating thanks to the control mechanism.
- The prototype's structure must sustain the loads under the previously described sailing conditions.
- The installation of the foiling device under no circumstances should compromise the structural integrity of the hull and other essential components of the Europe dinghy. Furthermore, the device must be removable and require little to no modifications of the hull and other components.

2.4. Background

A hydrofoil is a wing designed to operate in water. The higher viscosity and density of the medium allows an increased lift generation with a much smaller surface area than conventional wings. In boats, hydrofoils are used to raise the hull above the water, drastically reducing the drag, increasing at the same time efficiency and overall speed.

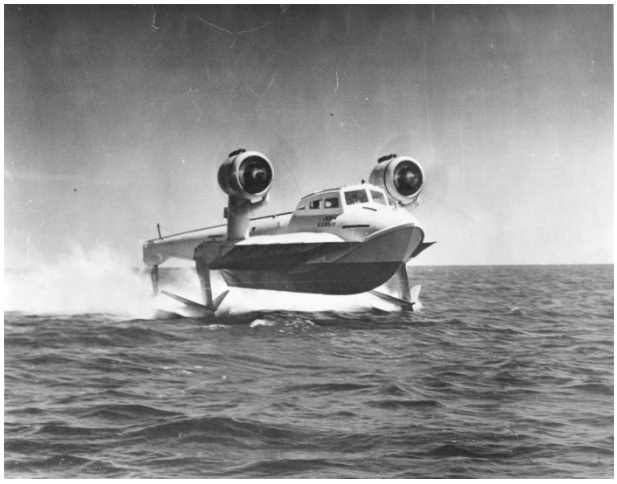

Figure 1: US Navy's XCH-4 hydrofoil craft. [17]

This technology has seen multiple commercial and military applications since the beginning of the 20th century. Despite its evident advantages, not until the 21st century it started to become popular in the world of sailing and specifically, dinghy sailing thanks to the contributions of the MOTH class.

Dinghy sailing is a sport that consists of using the power of the wind to manoeuvre and command a usually small lightweight sailboat with a rigid hull where the crew or single patron seat on top. Many different dinghy classes exist around the world, the International Europe Class being one of them.

As mentioned above, recently foiling dinghy sailboats are starting to gain some popularity among the sailing community. The technology is completely transforming the sport making it more intense as the sailboats become faster and more complex to handle. New sets of regulations to enable closer one-design racing appeared giving birth to new foiling classes such as the WASZP class. However, purposely foiling dinghies came at a cost and therefore are not available to everybody. Another solution is to design foiling kits for existing classes, and that is what this project is aiming for: creating a kit for the International Europe Class dinghy that once installed can provide the foiling experience to the user without the need of buying a completely new vessel.

3. STATE OF THE ART

3.1. The Europe dinghy

The Europe is a single-handed racing dinghy designed in Belgium in 1960 by Alois Roland as a class legal Moth dinghy. The design later in 1976 evolved into its own one-design class when the ISAF (International Sailing Federation) granted the Europe dinghy international status.

Figure 2: lateral view of a Europe dinghy. [1]

In 1992 it was introduced to the Olympic Games as the Women's single-handed dinghy Class, a position which it maintained until 2008. Despite no longer being an Olympic class, the Europe dinghy remains very popular especially on the old continent where international events are organised annually. The Europe dinghy can absorb a wide range of body types thanks to its developmental rig, which allows a high level of trimming. This characteristic allows sailors to compete at the same level regardless of their physique.

3.1.1. Technical characteristics

The hull of the modern Europe is made of fibreglass and weighs 45 kg. If we consider the other components needed to sail, the value increases to 60 kg. Since the foils will be installed to the hull, the original blueprints of 1960 have been considered as well as measurements from the current rulebook to make a 3D model. All the dimensions for this project will be taken from the same.

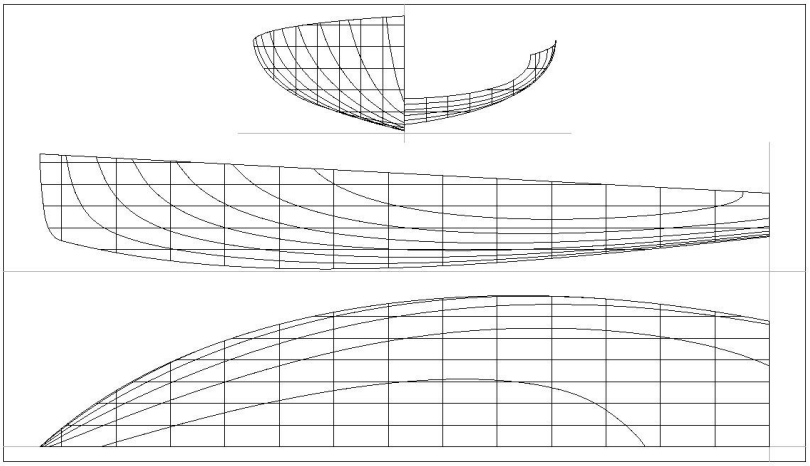

Figure 3: Europe dinghy hull blueprints used as a reference for the CAD model. [2]

It is important to know the weight of all the elements and the position of the centre of mass. Therefore, a list of all the components indicating its mass and position relative to the bow will be elaborated. Official documents from an existent Europe dinghy have been used to obtain the numerical values.

Element	Mass [kg]	Centre of mass position [mm]
Hull	45	1.744
Mast	5,55	647
Boom	3,25	647
Rudder blade	0,98	3.350
Rudder stock	1,27	3.350
Centreboard	2,80	1.606

Table 1: mass distribution of the Europe dinghy.

From here, we can obtain the position relative to the bow of the gravity centre.

$$\mathrm{Xcm} = \frac{w_h \cdot x_h + w_m \cdot x_m + w_{bo} \cdot x_{bo} + w_{bl} \cdot x_{bl} + w_{st} \cdot x_{st} + w_c \cdot x_c}{w_h + w_m + w_{bo} + w_{bl} + w_{st} + w_c} = 1.634{,}50\ \mathrm{mm}$$

If we consider the weight of the sailor to be $m_s = 80\ \mathrm{kg}$, and a normal position under normal sailing conditions (which will be discussed in more detail in further chapters) $x_s = 2900\ \mathrm{mm}$, we obtain the following centre of mass:

$$\mathbf{Xcm_t = 2.069{,}80\ mm}$$

3.1.2. Performance

Since a Europe dinghy solely uses the wind to create a forward force to move, it is important to know the effects that the wind direction and speed will have on the dinghy's behaviour. The main parameter which will affect the lift generation of the hydrofoils is the speed. Therefore, we have to study the effects that wind conditions have on the speed of the boat.

The sail of a sailboat operates as a vertical wing, generating a lift force that decomposes in the forward force and a lateral force which in the case of the Europe dinghy must be compensated by the weight of the sailor. Depending on the sailing direction, the angle of attack varies and the value of these forces is modified, as well as the position of the sail. We can assume that an experienced sailor achieves at all times an optimal weight distribution and sail trim. On the following diagram, we can observe all the possible courses of a dinghy sail.

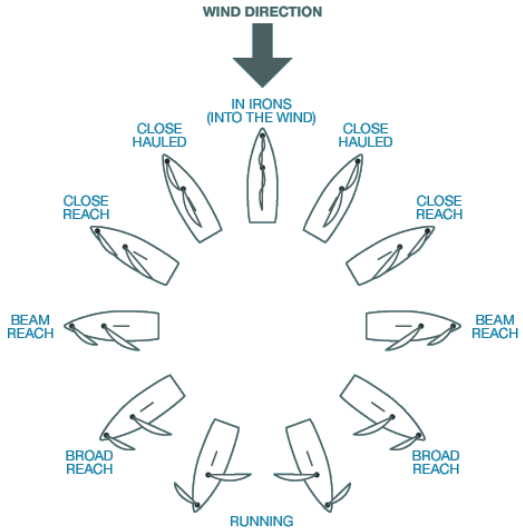

Figure 4: headings of a sailboat. [3]

A polar diagram indicating the boat speed function of the wind direction and intensity will be developed to study the behaviour of the dinghy under different wind conditions and headings.

We will use the GPS speed parameters of 4 different participants of the 2015 Europe Class YOUTH European Championship, publicly available at the TracTrac app [4]. We will measure the speed at four stages of the race corresponding to four different headings. Furthermore, three races developed under different wind intensities will be analysed. The App does not provide the value of the medium speed of the sailor during a determinate heading, so the following numbers correspond to a visual approximation

of the application's data. Also, we are neglecting the effect of the chop conditions, wind gusts and wind turbulence from other dinghies

Wind speed [km/h]	Sailor	Upwind [km/h]	Broad reach [km/h]	Beam reach [km/h]	Downwind [km/h]
42,6	ESP-805	7,9	18	16,8	16
	ESP-668	7,8	19	16	15,5
	ESP-631	8	19,4	16,8	16,6
	ESP-630	8,1	17,8	15,9	15,3

Table 2: performance under an average wind speed of 42,6 km/h.

Wind speed [km/h]	Sailor	Upwind [km/h]	Broad reach [km/h]	Beam reach [km/h]	Downwind [km/h]
27,78	ESP-805	8,6	15	15	14,3
	ESP-668	8,4	16,4	14,6	12,6
	ESP-631	8,8	16,8	14	11,1
	ESP-630	8,5	15,8	14,8	10,8

Table 3: performance under an average wind speed of 27,78 km/h.

Wind speed [km/h]	Sailor	Upwind [km/h]	Broad reach [km/h]	Beam reach [km/h]	Downwind [km/h]
14,82	ESP-805	7,4	10,6	11,3	8
	ESP-668	7,3	9,8	11,9	8,3
	ESP-631	7,1	10	10,9	7,8
	ESP-630	7,2	9,7	11	7,8

Table 4: performance under an average wind speed of 14,82 km/h.

With these values in mind, we can calculate the average speed of the Europe dinghy for the defined headings and elaborate the polar chart.

Wind Speed [km/h]	Upwind [km/h]	Beam reach [km/h]	Broad reach [km/h]	Downwind [km/h]
42,6	7,95	16,38	18,55	15,85
27,78	8,58	14,60	16	12,20
14,82	7,25	11,28	10,03	7,98

Table 5: average speed of the sailors in the different headings and wind conditions.

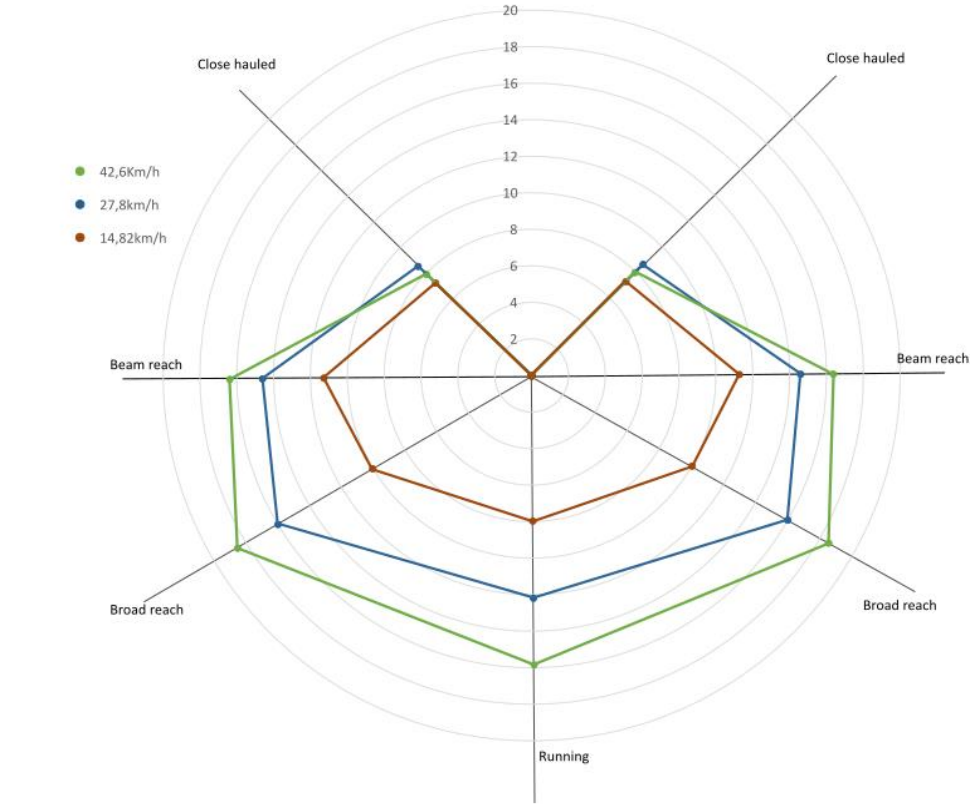

Figure 5: polar chart of the Europe dinghy.

Now, we will define the take-off at which the hydrofoils will generate sufficient lift to push the Europe's hull out of the water (**take-off speed**). The fastest headings are beam reach and broad reach. Therefore the take-off is considered as the average beam reach speed of the Europe dinghy at wind intensities of 10 knots, which is classified as a medium wind intensity. If we interpolate for this value, we obtain a dinghy speed of **5,44 knots, which is 10 km/h or 2,8 m/s.**

3.2. Introduction to hydrofoils

A hydrofoil is a wing designed to operate in water. In the boating industry, hydrofoils are used to provide lift for the vessel at a certain speed, usually near the maximum hull-borne drag, reducing the drag itself. Consequently, the boat can accelerate to a superior cruising speed, usually twice the take-off speed. Under these foiling conditions, the boat must be stable and controllable. This is achieved by introducing mechanical or electrical control mechanisms in a variety of configurations *(Costa* [5]*).*

3.2.1. History of hydrofoils

The hydrofoil technology appeared at the end of the 19th century, coinciding with the development of aircraft. The Mecham brothers were the first to try the concept by creating a flying boat on American soil. Similar prototypes saw the light in Europe, remarkably Enrico Foralini's concept from 1906. These machines aroused such an interest that even Alexander Graham Bell became involved in the technology. His associate Casey Baldwin and himself began designing and testing numerous prototypes. Inspired by Enrico Forlanini's ideas they built the HD-4 which in 1919 broke the water speed record *(Vellinga* [6]*).*

Despite this rapid development, hydrofoils did not see commercial applications until the end of WW2, when the technology was mature enough thanks to the developments in the aerospace industry and the understanding of foil behaviour. The public began to perceive hydrofoils as a much faster alternative to conventional boats. The German engineer Hanns von Schertel established in Switzerland the Supramar Company which in 1952 launched the first commercial hydrofoil, the PT10. Soon, the company was selling its product all around the world. During the same period, the Soviet Union rushed the development of hydrofoils both for civilian and military applications. It was believed that thanks to their superior mobility, speed and supposed immunity to torpedoes, hydrofoils would end up replacing conventional boats. However, the serious drawbacks of the hydrofoil configuration became evident and soon its popularity declined. Most of the militaries abandoned their programs and nowadays, only a handful of hydrofoil vessels are operating in commercial routes, mostly in rivers or lakes.

The technology is sensitive to surface objects impacts. Also, the cost of manufacturing is superior to its conventional counterparts, as well as its maintenance, which is also more complex. Moreover, their speed is no match to that of a modern airliner, rendering the technology useless for intercontinental travel.

Recently hydrofoil popularity has risen again in the sailing world, where speed and efficiency matter the most. Vessels with hydrofoils have substituted the conventional boats in America's cup vastly improving the spectacle of the race. To put into perspective, the AC75 hydrofoil boat class introduced for the 2021 cup can achieve speeds of over 50 knots or 92,6 km/h while the conventional vessels used in the 2017 edition achieve speeds of 12 knots or 22 km/h. In the same manner, foiling single-handed dinghies have recently appeared as new classes, such as the WASZP class, a derivative from the also foiling MOTH, which are replacing the conventional, much slower, single-handed dinghies like the Europe.

Figure 6: foiling AC75. [7]

3.2.2. Hydrofoil configuration

Hydrofoils exist in a large variety of shapes and sizes, but generally, a hydrofoil vessel must incorporate a forward lifting surface and an aft lifting surface for longitudinal stability. The loads do not have to be equally distributed. Alternatively, in a canard configuration, the forward foil acts as the stabilizer.

To provide stability and maintain a constant lift the principle of variable-area stabilization is used through **surface piercing hydrofoils**. This early configuration can be incorporated using V or W shape hydrofoils and does not require any mechanical or electrical control system. However, this configuration is sensitive to waves and thus it can only operate under certain conditions. An alternative is to **submerge** both lifting surfaces. With this distribution, the effects of wave height are mitigated but it must incorporate a variable incidence foil or flap control to provide the necessary stability.

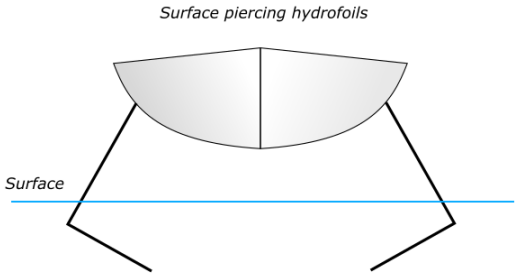

Figure 8: front view of a vessel equipped with surface piercing hydrofoils.

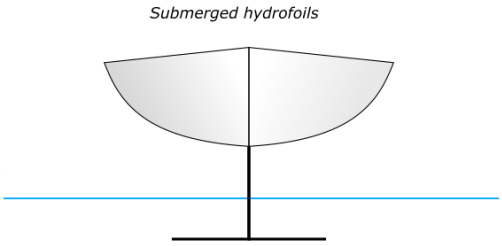

Figure 7: front view of a vessel equipped with submerged hydrofoils.

3.2.3. Single-handed foiling dinghies

- **MOTH**

The same development class that gave birth to the Europe has become a high-performance foiling class, the International MOTH. The design restrictions of this class are lax, allowing the manufacturers to introduce innovations and test new concepts. It is considered the most extended foiling class of today as well as the fastest single-handed dinghy in the world.

Figure 9: MOTH. [8]

The MOTH uses a double submerged foil configuration. The main central foil, situated at the middle of the hull, forward to the sitting position of the sailor, provides a large portion of the lift. The rear hydrofoil, which also acts as a rudder, also provides positive lift, stabilizing the configuration. The front foil incorporates a mechanical flap linked to a wand that hangs from the bow of the dinghy. The wand measures the proximity of the waterline and automatically adapts the lift of the main foil, thus maintaining a constant ride height.

- **WAZP**

The WASZP is the cheaper alternative to the MOTH and therefore the design is very similar. Given its competitive price, this class is rapidly expanding and currently, international events are held all over the globe.

Figure 10: WASZP. [9]

3.3. Introduction to hydrodynamics

Hydrodynamics is defined as the branch of physics that deals with the motion of fluids and forces acting on solid bodies immersed in fluids relative to them *(Merriam-Webster* [10]*).* The definition is nearly equal to that of aerodynamics, and essentially hydrodynamics is nothing more than underwater aerodynamics. However, we have to consider two phenomena of major importance not present in aerodynamics due to the nature of air: cavitation and ventilation.

- **Cavitation:** Cavitation is a phenomenon that occurs when the pressure reduction of the upper surface of the foil is great enough to cause the flowing water to vaporise. A cavity filled with gas is created and most of the lift generated by the foil is lost. When the gas cavity collapses further down the chord, the water strikes the foil surface producing vibrations, noise and even damaging it. This phenomenon only occurs at sufficiently high speeds and therefore it will not be considered during this project. *(Costa* [5]*).*
- **Ventilation:** Ventilation occurs when air is introduced into the upper surface of the foil, disrupting the flow of water and reducing the generated total lift. Lifting surface-piercing foils are very susceptible to ventilation due to wave disturbances.

3.3.1. The Free surface

Apart from the phenomena explained above, we have to consider another difference between aerofoils and hydrofoils, which is the proximity to the air-water interface. When a hydrofoil operates near the surface, it is more likely the introduction of air bubbles that

can disrupt the generation of lift. In addition, since less water is displaced by the upper surface of the foil, less mass is vertically accelerated and thus the generated lift is reduced. The relation between the proximity to the surface and the lift generated by a hydrofoil is expressed as the **submergence factor**. Beason and Buckle's formula defines this factor as:

$$F_s = 1 - 0{,}222\left(\frac{1{,}5 \cdot c - h}{c}\right)^2 \qquad (1)$$

Where c is the profile's chord and h the depth of operation.

This factor multiplied by the generated lift under normal conditions gives us the modified value. The following graph represents the F_s for various depths of a hydrofoil in units of chord.

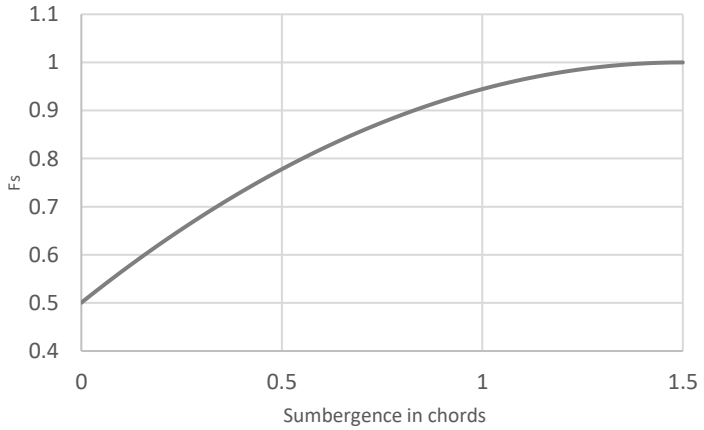

Figure 11: submerge factor per unit of depth in chords.

As shown in *Figure 11*, for depths of more than 1,5 chords the effects on the generated lift are negligible.

3.4. Aerodynamics of a wing

As previously discussed, hydrofoils can be studied as wings that operate underwater. Therefore, during the development of this project, some wing theory will be used to size the foiling surfaces and obtain their characteristics.

3.4.1. Profile aerodynamics

In this subsection, an introduction to the aerodynamics of wing profiles will be given.

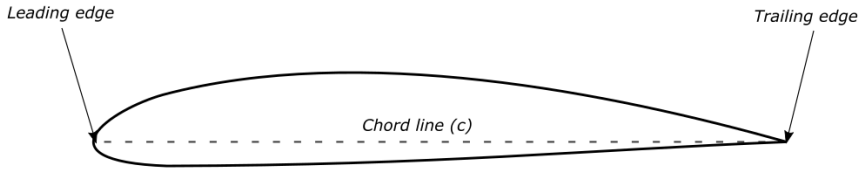

Figure 12: basic geometry of an aerofoil, wing profile or aerodynamic profile.

When an aerodynamic profile is under a fluid stream, due to the Coanda effect this fluid will flow attached to the surface of the foil. Due to the geometry of a wing profile, this flow at the trailing edge is diverted downwards onto the departing airstream. Through the 3rd Newton-Law, a force will be created upon the profile as well as a moment. This force is later decomposed into lift and aerodynamic drag, while the moment receives the name of pitching moment. This phenomena also creates a lower-pressure area at the upper surface of the foil and a high-pressure zone at the lower surface. This uneven distribution of pressures is sometimes also used to explain the creation of aerodynamic forces around the foil.

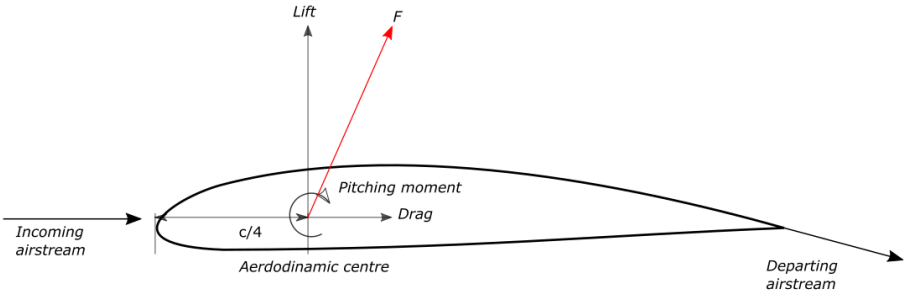

Figure 13: forces acting on the aerodynamic centre of an aerofoil.

3.4.2. Boundary layer

In aerodynamics and fluid mechanics, we cannot neglect the effects of fluid viscosity since it is responsible for the apparition of friction forces. An ideal fluid (without viscosity) flows over the solid and has a finite velocity. However, in reality, the speed over the surface is zero, creating a thin region in which a velocity gradient exists. This receives the name of the boundary layer. Therefore, when a fluid flows over a surface we can distinguish between the free stream zone, where the viscous forces are neglected and the boundary layer, where they have significant importance. The direction of the generated viscous stresses is the same as the fluid movement, slowing the fluid stream. There exist two types of flow in a boundary layer:

- **Laminar boundary layer**

This type of boundary layer is developed under smooth flow. It is thinner than the turbulent boundary layer and the gradient is less pronounced, hence it generates less friction. However, it is unstable and can easily transition into a turbulent one as it increases its thickness.

- **Turbulent boundary layer**

A turbulent boundary layer has more energy than a laminar one, and therefore it is more stable. However, it implies that more friction is generated.

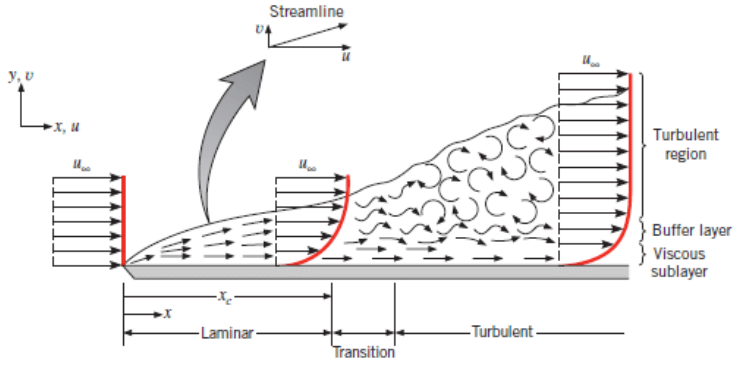

Figure 14: boundary layer development. [11]

To know whether a boundary layer is laminar or turbulent over a wing profile we use the dimensionless Reynolds number

$$\mathrm{Re} = \rho \cdot u_\infty \cdot \frac{c}{\mu} \qquad (2)$$

If $\mathrm{Re} \leq 3 \cdot 10^6$ the flow is considered laminar. Otherwise, we say that the flow is turbulent.

3.4.3. Boundary layer detachment

The line of the chord of a wing profile can have a certain angle to the relative airflow. This angle is called the angle of attack (α). The variation of this angle has a direct effect on the forces generated. An excessive angle of attack generates an adverse pressure gradient which can detach the boundary later by lowering its energy and finally inverting its flow. When this happens, the natural pressure distribution of the aerofoil is compromised, the lift significantly decreases and the aerodynamic drag increases.

3.4.4. Aerodynamic coefficients

The dimensional analysis in aerodynamics and fluid mechanics plays a very important role since it allows us to describe a physic phenomenon with a reduced number of variables. Hence, instead of studying the direct dependency between lift, drag, pitching moment and the contour variables, we work on aerodynamic coefficients. These coefficients are the only function of the Reynolds number (Re), the Mach number (Ma) and the angle of attack *(Franchini* [12]*).*

- Lift coefficient:

$$C_l = \frac{L}{\frac{1}{2}\rho u_\infty^2 c} \tag{3}$$

- Drag coefficient:

$$C_d = \frac{D}{\frac{1}{2}\rho u_\infty^2 c} \tag{4}$$

- Free moment coefficient:

$$C_{m1/4} = \frac{M}{\frac{1}{2}\rho u_\infty^2 c^2} \tag{5}$$

3.4.5. Lift coefficient

To express the behaviour of a wing profile, normally we study the variation of the three mentioned coefficients for the angle of attack. In the case of the lift coefficient, it increments linearly with the angle of attack. This linear section of the curve can be represented as:

$$C_l = C_{l\alpha}\alpha + C_{l\alpha 0} \tag{6}$$

If the wing profile is symmetric, when $\alpha = 0°$ the pressure distribution is also symmetric and therefore $C_{l\alpha 0} = 0$. On the other hand, if the profile presents curvature, it is verified that $C_l \neq 0$, and then the angle in which $L = 0$ is designated as α_0.

After the mentioned linear zone, the C_l increases until it reaches a maximum denominated $C_{l,max}$ which is achieved at an angle $10° < \alpha_s < 15°$. For superior angles of attack, the lift coefficient decreases, and at a certain point the profile stops generating lift, phenomena associated with the previously explained boundary layer detachment.

The Reynolds also influences the lift coefficient. As the Reynolds increases, the value $C_{l,max}$ is incremented. Therefore for superior Reynold numbers, the profile presents a better stall behaviour.

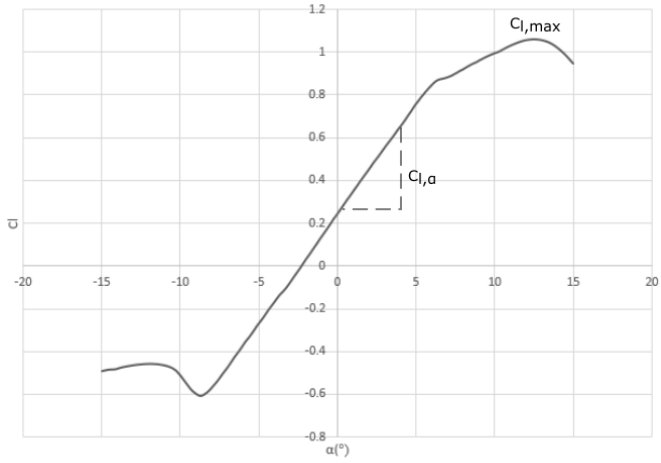

Figure 15: C_l plot of a wing profile.

3.4.6. Drag coefficient

The behaviour of the drag coefficient C_d is described by a polar curve. This polar curve can be approximated by the parabolic expression:

$$C_d = C_{d,min} + k \cdot \left(C_l - C_{l_{cd,min}}\right)^2 = C_{d0} + jC_l + k \cdot C_l^2 \qquad (7)$$

The values of the C_d coefficient are always positive, and it presents a minimum value, $C_{d,min}$ for attack angles between 0° and 4°. When the profile stalls, the drag drastically increases and the polar no longer resembles a parable. For larger Reynolds numbers the branches of the parable present less convexity. C_{d0} is the parasite drag coefficient

and represents the friction drag forces. k and j are given values which can be obtained from the appropriate reference, but the methodology is out of the scope of this project.

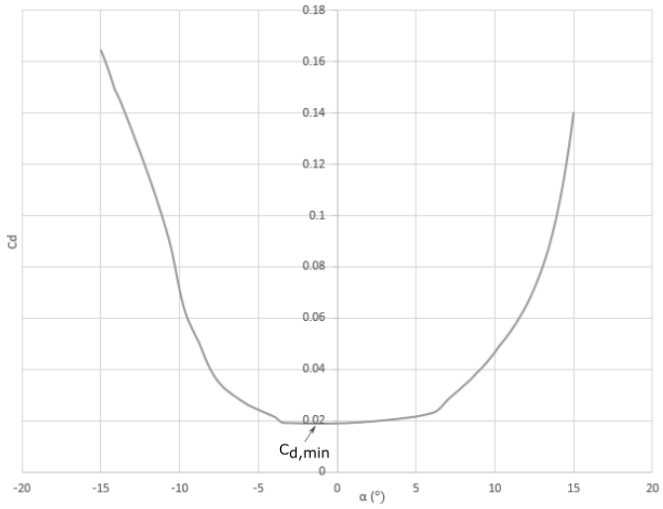

Figure 16: Cd polar.

3.4.7. Moment coefficient

Normally, we study the variation of the wing profile moment at ¼ of the profile's chord to the angle of attack. All aerodynamic profiles present negative aerodynamic coefficients, which indicates that an anti-clockwise moment is generated. A wing profile generates a constant moment independent of the angle of attack and a moment inversely proportional to the angle of attack, denominated m_0 and m_α respectively.

3.4.8. Three-dimensional wing

The previously discussed points refer to the aerodynamics of bi-dimensional wing profiles. When studying three-dimensional wings of finite spans, the fluid behaves differently. It has been explained that the pressure difference between the upper and lower surface of a wing generates lift. However, in a finite wing, this pressure imbalance makes the flow at the lower surface curve onto the low-pressure zone at the upper surface, generating a circulatory motion or a trailing vortex. These vortices induce a small velocity component in the downward direction of the wing, called downwash.

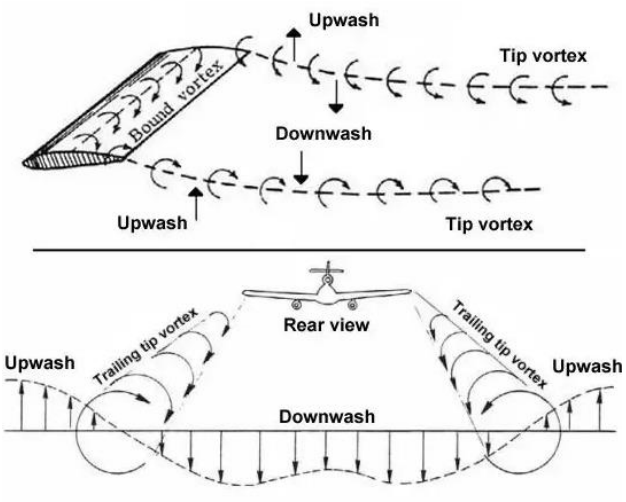

Figure 17: depiction of the trailing vortices and the generated downwash. [13]

This downwash is combined with the freestream velocity, creating a local relative wind and an induced angle of attack. Therefore, the angle of attack seen by the local aerofoil section is the angle between the chord line and the local relative wind, the effective angle of attack. In addition to that, drag is generated due to the presence of the downwash. This drag is defined as induced drag.

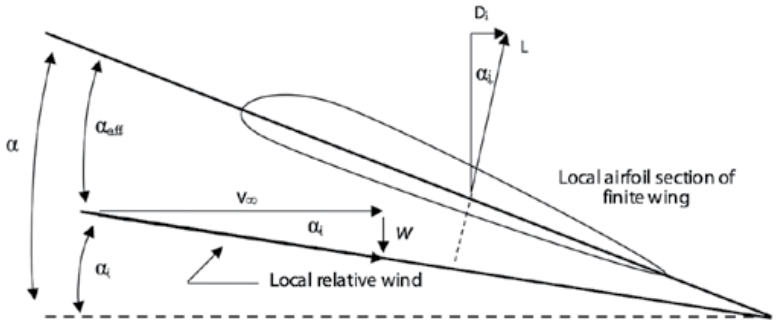

Figure 18: illustration showing the variations produced by the induced downwash. [14]

3.4.9. Three-dimensional lift coefficient

The lift coefficient of a three-dimensional wing is denominated C_L and expressed as:

$$C_L = \frac{L}{\frac{1}{2}\rho u_\infty^2 S} \tag{8}$$

As well as the lift coefficient for a wing profile, there is an angle of attack range for which it presents a linear behaviour. Therefore, $C_L = C_{L\alpha}(\alpha - \alpha_0)$, being $C_{L\alpha}$ the slope of the

equation, α the wing's angle of attack and α_0 the angle of attack for which the lift is null. The fact that the lift generated by a wing is inferior to the one generated by the equivalent profile is represented by a smaller slope. The Prandtl theory approximates the three-dimensional lift slope based on the bi-dimensional value and different parameters of the wing. For an elliptical platform, which is considered the most efficient three-dimensional wing shape, the slope of the lift curve:

$$C_{L\alpha} = \frac{C_{l\alpha}}{\left(1 + \frac{C_{l\alpha}}{\pi\Lambda}\right)} \qquad (9)$$

Λ is known as the aspect ratio or AR of the wing, and is defined as $\Lambda = b^2/S$, where S is the wing's surface and b its span. For greater aspect ratios, the value $C_{L\alpha}$ will be closer to $C_{l\alpha}$.

For wings without an elliptical shape, we have to incorporate to the expression the Oswald efficiency number e. This is a correction factor that depends on the aspect ratio and shape of the wing. Typically its range is between 0,7 and 0,85. Therefore, the generic expression of the lift curve slope for a three-dimensional wing is:

$$C_{L\alpha} = \frac{C_{l\alpha}}{\left(1 + \frac{C_{l\alpha}}{\pi\Lambda}\right)} e \qquad (10)$$

3.4.10. Three-dimensional drag coefficient

The three-dimensional drag coefficient is defined as:

$$C_D = D/(1/2 \cdot \rho \cdot u_\infty^2 \cdot S) \qquad (11)$$

As mentioned before, the induced downwash generates an induced drag, as shown in *Figure 18.* This can be expressed in terms of lift, $D_i = L\alpha_i$. The induced angle of attack can be expressed as $\alpha_i = C_L/\pi\Lambda$, and the lift can take the form of $L = C_L \cdot 1/2 \cdot \rho \cdot u\_\infty^2 \cdot S$. Then:

$$D_i = \frac{1}{2}\rho u_\infty^2 S \frac{C_L^2}{\pi\Lambda} \rightarrow C_{Di} = \frac{C_L^2}{\pi\Lambda} \quad (12)$$

If we want to achieve smaller induced drags we have to build a wing with a high aspect ratio. The previous expression is valid again for elliptical platforms since they have a constant induced angle of attack for all its span. For generic wing shapes, we have to one more time introduce the Oswald efficiency number to the expression and, therefore, they present higher induced drags. If we also add to the expression the friction drag we obtain the total drag coefficient formula.

$$C_D = \frac{C_L^2}{\pi\Lambda e} + C_{d0} \quad (13)$$

3.4.11. Three-dimensional moment coefficient

The last of the aerodynamic coefficients it's not of particular interest when studying three-dimensional wings. The only thing that can be said about it is the addition of the wing's surface instead of the chord on the non-dimensionalization of the parameter,

$$C_{M1/4} = M/(1/2 \cdot \rho \cdot u_\infty^2 \cdot c \cdot S) \quad (14)$$

What is more relevant in three-dimensional wings is the study of moments of an overall wing-tail configuration with respect to its centre of masses, which is crucial to study its stability. This will be commented further below in *chapter 3.5.*

3.4.12. Wing platform

We have mentioned the existence of the **elliptical wing** platform, which is defined as the most efficient wing shape. It presents a constant downwash throughout the wing as well as the induced angle of attack. Hence, it has the smaller induced drag of all wing platforms. Its lift distribution is known as elliptical lift distribution, where the root profiles generate a greater lifting force than the ones situated at the tip, diminishing the generation of bending moments that could compromise the structural integrity of the

wing. Despite this favourable lift distribution, when the aeroplane stalls, the first section that stops generating lift are the tips, where the control surfaces are normally located. In addition, this geometry is difficult to manufacture. The alternative is producing a **tapper wing** platform, easier to manufacture and its lift distribution is close to the elliptical one, although not as good. The higher the tapper ratio, the more will the wing performance resemble an elliptical. Finally, **rectangular wing** platforms have the worst aerodynamic performance of all the platforms. However, it has the advantage that the tips do not stall, making them more forgiving in emergencies. Also, some commercially available submerged hydrofoils dinghies such as the WASZP use this platform since the profile can be extruded using aluminium, making it easier and cheaper to manufacture than the other alternatives.

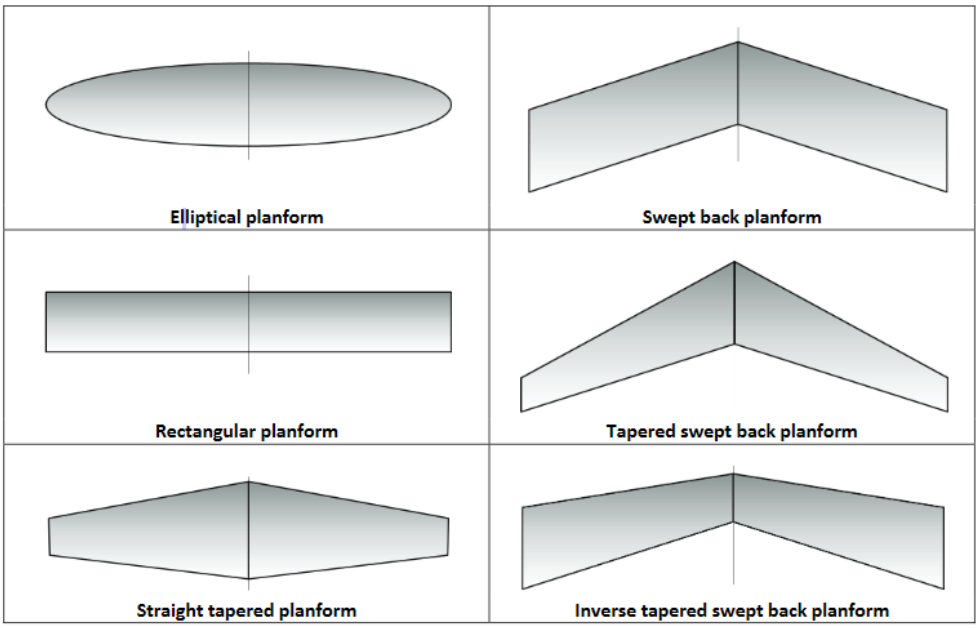

Figure 19: wing platforms.

3.4.13. Wing architecture

Multiple parameters interfere with the definition of a wing geometry. Previously we have defined the AR of a wing, as well as the chord and span. The last two concepts are represented in the following figure.

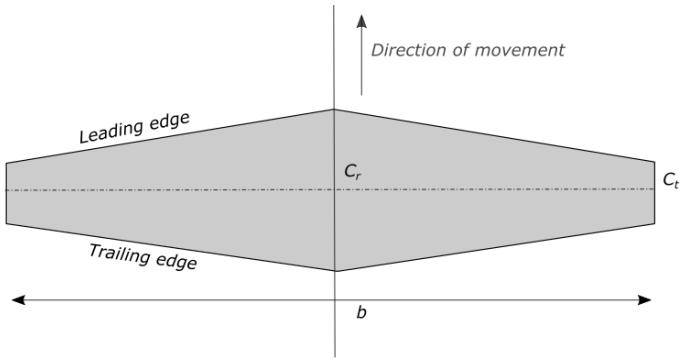

Figure 20: geometry of a wing.

Other important parameters that we must contemplate when sizing a foil are the following:

- The **swept angle** or φ is defined as the angle between the line that goes through the 25% of the chords along the span and the line perpendicular to the root chord.
- The **dihedral angle** δ is the angle between the horizontal plane which contains the root chord and the medium plane between the top surface and the bottom surface of the wing.
- The **twist** can be geometrical or aerodynamic. The geometrical twist θ_g is defined as the angle between the profile chord and a reference chord, normally the one of the root profile. On the other hand, the aerodynamic twist consists of variating the profile shape along the span of the wing.

3.5. Stability

In this section, the longitudinal stability of plane configurations will be explained. This theory can be also used in hydrofoil configuration like in our case study. The stability of a plane is a property related to the equilibrium state, and it studies the behaviour of the aeroplane when one of the variables which define the equilibrium state is perturbed. When studying the equilibrium of a wing-tail configuration the effects of the control surfaces are neglected. With that being said, we first have to distinguish between two types of stability: static and dynamic. The first one refers to the initial reaction of the aeroplane in front of perturbations under stable flight. The second one refers to the evolution of the equilibrium variables after the initial perturbation.

3.5.1. Longitudinal equilibrium

The longitudinal equilibrium is the study of the equilibrium state neglecting the lateral and directional variables. The equations that define such equilibrium are moments and forces characterized on the lateral plane of the aeroplane or hydrofoil. These equations are the following:

$$\sum \mathrm{F} = 0 \tag{15}$$

$$\sum \mathrm{M_{cm}} = 0 \tag{16}$$

If the sum of all the forces acting on the configuration is equal to 0 and the sum of all the moments on the centre of mass is also null then at that moment the configuration is under longitudinal equilibrium. However, it does not mean that it will be statically stable nor dynamically stable.

3.5.2. Static stability

As mentioned above, when talking about static stability, we are referring to the study of the moments and forces that appear on the aeroplane immediately after the incidence of a perturbation such as a wind gust. If the resultant forces amplify the perturbation, we say that the configuration is **statically unstable** whereas if they mitigate the effects of the perturbation the configuration is **statically stable**. Finally, if the perturbation effects are not amplified nor mitigated we have **neutral static stability**.

For the study of the static stability of a configuration we often make use of the non-dimensional global moment coefficient, which is expressed as:

$$\mathrm{C_{M,cm}} = \sum \frac{\mathrm{M_{cm,y}}}{\frac{1}{2}\rho \mathrm{u_\infty^2 S\bar{c}}} \tag{17}$$

Note that we are taking as reference all the moments acting over the configuration with respect to the centre of mass. If we further develop the expression we obtain:

$$C_{M,cm} = C_{M0} + C_{M\alpha} \cdot \alpha + C_{M\delta_e} \cdot \delta_e \quad (18)$$

Where C_{M0} is the moment coefficient independent to the angle of attack, $C_{M\alpha}$ is the derivative of the moment coefficient of the configuration with respect to the angle of attack, $C_{M\delta_e}$ is the derivative of again $C_{M,mc}$ to δ_e, which is defined the deflexion angle of the elevator.

If we plot this expression in terms of α, we obtain a graph that characterises the stability of the configuration. The intersection point with the x axis indicates the angle of attack for which we have longitudinal equilibrium. Moreover, the sign of $C_{M,cm}$ can give us an idea of the type of static stability. A positive value of $C_{M,mc}$ indicates that if a perturbation increases the angle of attack, the resulting moment will do the same, further increasing the effect of the perturbation. Therefore, these circumstances, the configuration will be instable. On the other hand, if $C_{M,cm} < 0$ the opposite happens, indicating a stable configuration. Finally, if $C_{M,cm} = 0$, the configuration is neutral.

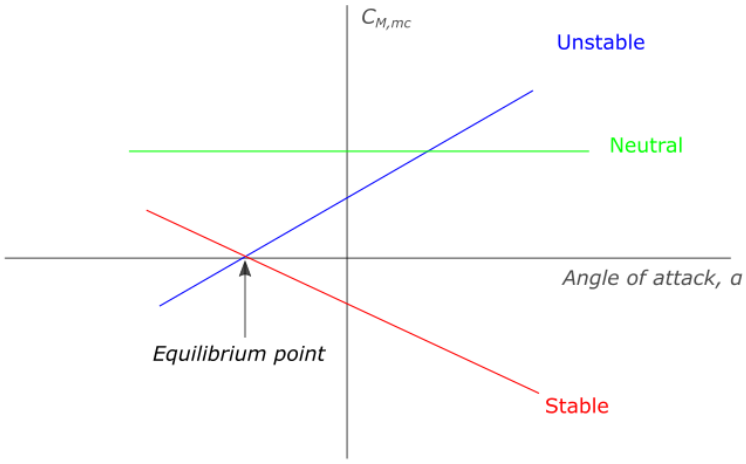

Figure 21: static stability plots.

3.5.2.1. Influence of the centre of mass position

We know that for a configuration to be statically stable, $C_{M,cm}$ must be negative. Among other parameters, this coefficient is related to the position of the centre of mass. In a foiling dinghy, the position of the sailor is constantly adapted to achieve the longitudinal equilibrium. There exists a sitting position for which $C_{M,cm} = 0$ and it receives the name of neutral point. If the sailor positions itself in front of this point, the configuration becomes stable but the angle of attack that guarantees equilibrium decreases. On the other hand,

if the sailor delays its position behind the neutral point the configuration becomes unstable and the equilibrium angle of attack increases.

3.5.3. Dynamic stability

As previously announced, dynamic stability studies the time evolution of the flight variables, such as the angle of attack, when the equilibrium condition has been modified by a perturbation. A configuration is **dynamically unstable** when the variations produced by the perturbation are amplified through time. When the opposite situation occurs, we say that the configuration is **dynamically stable.** Finally, when the variables are not increased nor mitigated, the configuration is **dynamically neutral.**

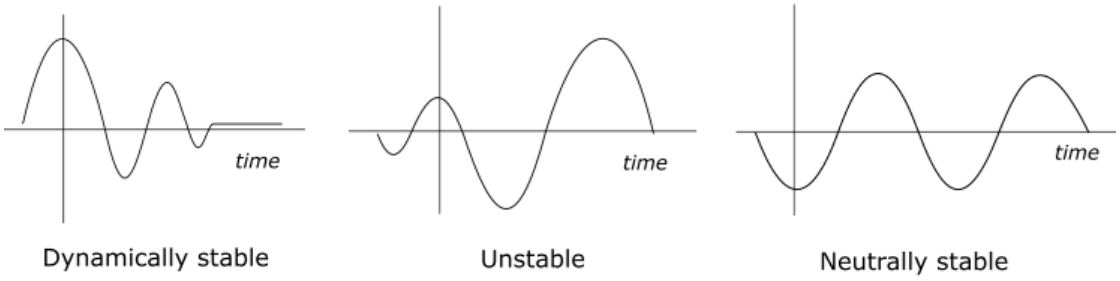

Figure 22: types of dynamic stability.

4. INITIAL SIZING

In this section, the initial concept will be defined through a mathematical study based on the explained theory. To begin, the selection of the initial configuration will be discussed. Afterwards, an aerodynamic and stability study will be presented in which the platform geometry, dimensions and overall characteristics are determined. Finally, the results will be validated using the XFLR5 software.

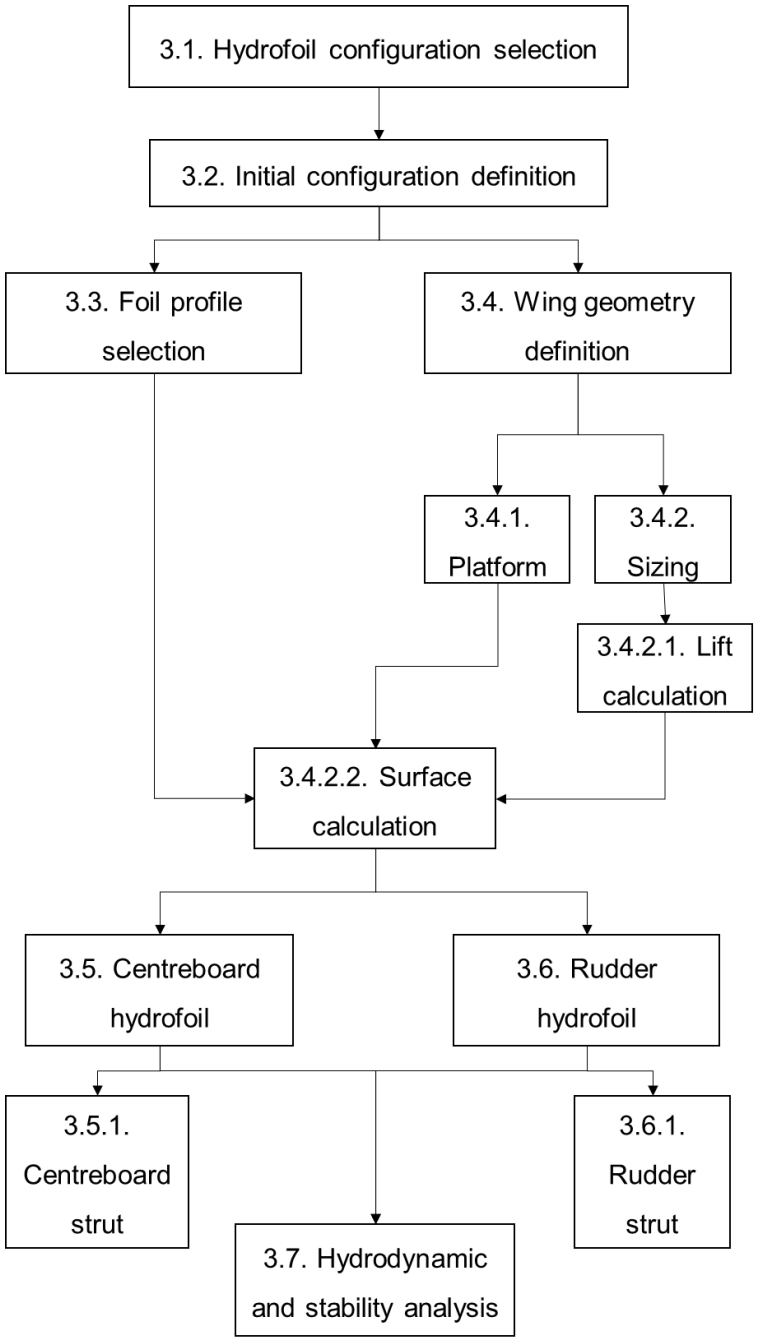

Figure 23: initial sizing process overview.

4.1. Hydrofoil configuration selection

Previously we discussed the existence of mainly two types of foiling configurations, surface piercing hydrofoils and submerged hydrofoils. The election of the appropriate platform involves the study of the advantages and disadvantages of both options as well as the study of similar designs and the objectives of this project. We will begin by listing the pros and cons of each configuration.

Platform	Pros	Cons
Submerged	Less susceptible to waves. Less foil area required.	Less stable. Require a control system.
Surface piercing	More stable, lift vector inclined toward the centre of gravity.	Susceptible to waves. Do not require a control system.

Table 6: platform comparison

Now, if we look back to the configurations adopted by single-handed foiling dinghies such as the MOTH, we can see that generally, they adopt a double submerged foil configuration. In addition, there exist some kits that allow the transformation of non-foiling dinghies into foiling ones without modifying their architecture. Such is the case of the Foiling Laser Kit. These kits also opt for a submerged configuration mainly because it allows the adaptation of the foils in existing structures of the hull. Therefore it can be said that the submerged configuration could be adopted without the need of modifying the hull.

Knowing the requirements of the design and the characteristics of the mentioned configurations, we will elaborate to take the final decision. We will assign a weight to all the criteria and the configurations will be rated for each category on a scale from 1 to 3. The one with the greatest final score will be the configuration to be used.

Criteria	Weight	Submerged		Surface Piercing	
	g	***p***	***gxp***	***p***	***gxp***
No invasive	10	3	30	1	10
Resists waves	8	2	16	1	8
Structural integrity	4	2	8	1	4
Simplicity	7	1	7	3	21
Stability	8	1	8	3	24
Manufacturing ease	8	3	24	1	8
SUM *(gxp)*	45		**93**		75
OWA			**0,69**		**0,56**

Table 7: decision making.

Based on the previous table results, a **double foil submerged** configuration has been chosen since it obtained the higher score.

4.2. Initial configuration definition

Since we will be using a double foil submerged configuration, we have to discuss where we will be allocating those foils. As mentioned above, the ideal configuration must be integrated into the existing structures of the dinghy. Therefore, it has been decided to allocate the central foil or **centreboard foil** in place of the centreboard and the rear foil or **rudder foil** attached to the rudderstock. The central foil will provide the majority of the lift while the additional force produced by the rear foil will stabilize the configuration. Moreover, the central foil will incorporate a flap to provide the extra stabilization needed on a submerged configuration, similar to the MOTH or WASZP concept. The following table shows the dimensions and flap sizes of eight MOTH hydrofoils, manufactured by different companies.

		Fasta-craft	**Fasta-craft Gen.2**	**Blade-rider**	**Hungry Beaver**	**Full force**	**Nick Flutter**	**Phil Stevo**
Main foil	**Flaps**	Foil trim	Foil trim	30% flap	30% flap	30% flap	33% flap	30% flap
	Span [mm]	900	850	990	985	860	880	880
	Chord [mm]	120	120	117	122	110	120	124
Rudder foil	**Flaps**	-	-	-	-	-	25% flap	-
	Span [mm]	600	650	830	878	700	650	650
	Chord [mm]	120	120	100	114	110	120	124

Table 8: MOTH hydrofoils from different manufacturers.

We can see that most of the manufactures decided to install a **30% chord flap** through all the span of the main foil. Generally, a flap of this size deflected 30° increases the C_L of the wing thus permitting cruise speeds of nearly twice the take of speed.

4.3. Foil profile selection

In this section, the profiles to be used in the centreboard foil and rudder foil will be selected. Since both of the foils have to produce positive lifts and must operate under the same conditions, it has been decided that both of the hydrofoils will use the **same wing profile.**

First of all, we will calculate the Reynolds number to give an idea of the conditions of operation, taking as a reference the properties of seawater, a take-off speed of 2,8 m/s and a chord of 0,2 m. We will be using *eq.(2).*

$$\mathrm{Re} = \frac{1.024 \cdot 2{,}8 \cdot 0{,}2}{0{,}00098} = 585.142{,}85 < 3 \cdot 10^6$$

The previous number indicates that the flow around the foils will be laminar. Therefore it is convenient to use profiles designed to operate under laminate flows such as the NACA 6-Series, to reduce the overall drag. To select the appropriate profile, we will compare the drag of different profiles and the lift achieved at minimum drag conditions. These profiles are the **NACA-63-412**, the **Eppler 393,** the **Wortmann FX60-100** and the **Eppler 817** have been chosen for this analysis since they all have been previously used in hydrofoil construction. The study will be conducted using the XFLR5 software.

The drag polar chart of each profile for a Reynolds number of 550.000 are the following:

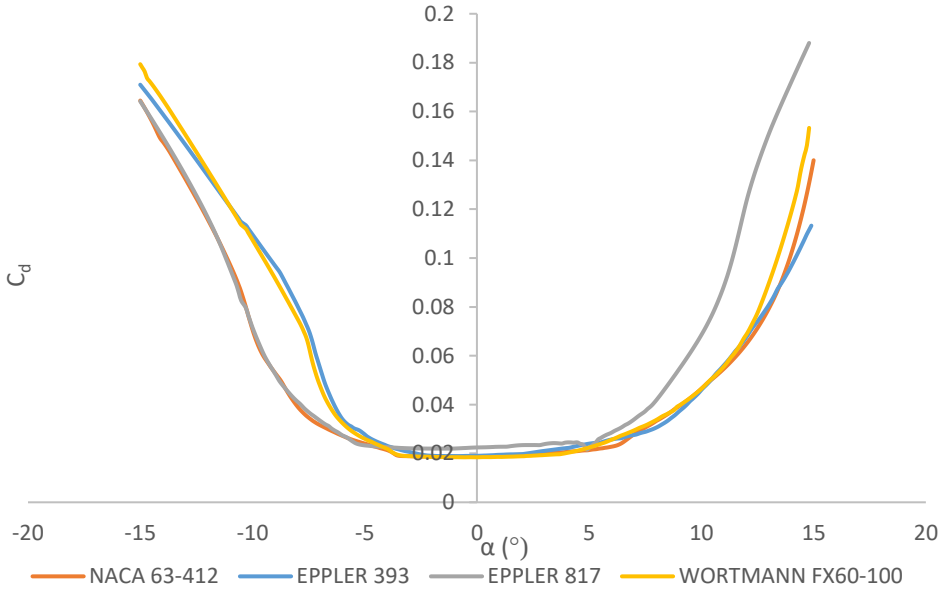

Figure 24: drag polar chart.

Doing the same for the lift coefficient we obtain:

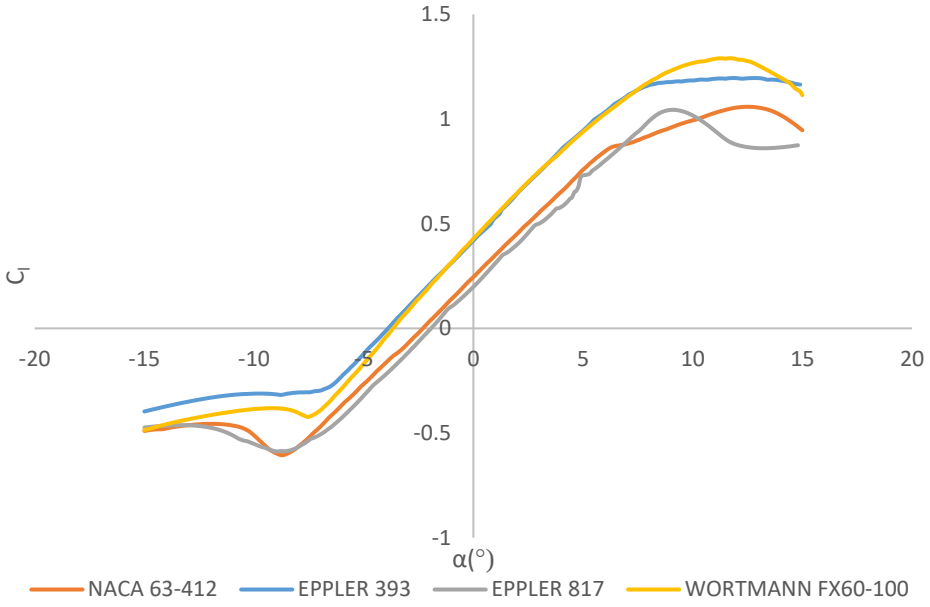

Figure 25: lift representation.

From *Figure 24*, the NACA 63-412 along with the EPPLER 393 and the FX60-100 presents a fairly good C_d behaviour for positive angles of attack. However, for negative angles of attack, the performance of the last two is inferior to the NACA 63-412. On the other hand, the FX60-100 and the EPPLER 393 can generate the more lift than the NACA 63-412.

At this point, either of these three options could be considered as viable. However, a thicker profile would be preferable since it is easier to manufacture. The following figure represents the geometry of the 3 candidate foils. (In blue, the NACA 63-412, in red, the EPPLER 393 and in green, the FX60-100).

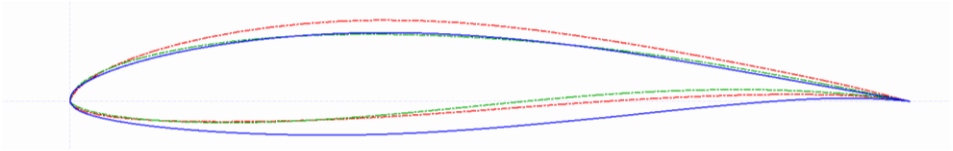

Figure 26: comparison between the 3 wing profiles.

We will choose the **NACA 63-412** as our profile platform since it presents more thickness at the trailing edge than its counterparts.

Moreover, the fixed angle of attack at which the hydrofoil will be manufactured has to be indicated. The NACA 63-412 achieves minimum drag at 1°. Also, at this angle, the profile achieves a high C_l. Therefore it has been decided that for both the centreboard foil and the rudder foil the fixed angle of attack or **intrinsic angle of attack** will be 1°.

4.4. Wing geometry definition

Both the centreboard and rudder hydrofoil will present similar geometries since, as mentioned above, they must operate under the same conditions. In this section, the most appropriate shape for these hydrofoils will be discussed. Further below the dimensions will be defined according to the required lift.

4.4.1. Platform

As previously discussed in *Wing platform*, the most efficient shape that our hydrofoils could adopt is elliptical. However, it would be difficult to manufacture. Hence, it has been decided to use a tapered platform in both centreboard and rudder foils to resemble the performance of an elliptical platform while optimising the manufacturing process.

4.4.2. Sizing

In this section, we will define the necessary surface area of the centreboard and rudder hydrofoils which will ensure stable flight. *Equation (15)* and *eq.(16)* define the longitudinal stability of a hydrofoil configuration. Hence, we must define all the forces acting on the foiling Europe dinghy under stable flight and solve the system of equations to obtain the values of L_1 (lift generated by the centreboard hydrofoil) and L_2 (lift generated by the rudder hydrofoil). Once we determined these values, using the explained wing theory we will elaborate a mathematical model to determine a curve of wing surface vs. water stream for the obtained lifts. The intersection of the curve with a speed of 2,8 m/s which if we remember is defined as the take-off speed will give us the necessary surface for the hydrofoil under study.

4.4.2.1. Lift calculation

Firstly, it is important to define the position of the sailor to the bow, since the hydrofoils must be able to provide sufficient force to lift the dinghy with the sailor. The mass centre of the dinghy has already been defined in *chapter 3.1.1.* Considering that an average sailor fully equipped weights about 80 kg and typically sits at 2,39 m behind the bow, we can obtain the total mass centre position by repeating the calculations with the added mass, giving us a value of $\mathbf{Xcm_s = 2,065\ m.}$ (see *subsection 3.1.1*)

The position of the hydrofoils has already been defined, and with it, the location of the lifting forces: the centreboard hydrofoil will sit in place of the centreboard and the rudder hydrofoil will be attached to the rudder stock. Hence, they will be located at 1,4 m and 3,35 m behind the bow, respectively.

Apart from the masses and the lifting forces we also have to consider the wing pressure over the sail. Being a triangular shape, we can approximate its centre of pressure location at about 1/3 of its height. The sail produces a longitudinal force that moves the dinghy forward and a lateral force that tilts it on the longitudinal axis. The sailor has to provide a counterweight if he does not want the boat to tip over. Therefore, under ideal conditions, it will sit on the opposite side of the sail.

Now that we know that the sail forces can be decomposed into a longitudinal and a lateral force, and the last one is compensated by the weight of the sailor, we have to study the effects of the first component. Since it is located at a certain height, it generates a moment that has to be incorporated into the study. Hence, it is important to obtain the total force of the sail. One methodology would involve a complex CFD study. The other option consists of obtaining the lateral force based on the sitting position of the sailor, and knowing the angle of incidence of the wind and the opening of the sail we can find the longitudinal force and the wanted moment. We will follow the last approach.

Under the sailing conditions defined in *3.1.2* we have the following schemes in which the sitting position of the sailor and angle of the sail are defined:

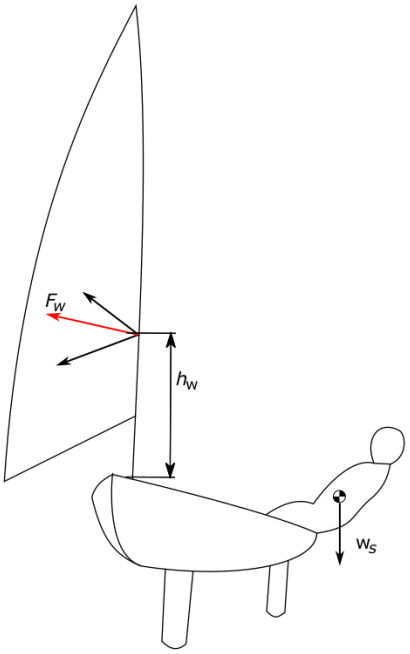

Figure 28: top view of the sailor position and sail centre of pressure.

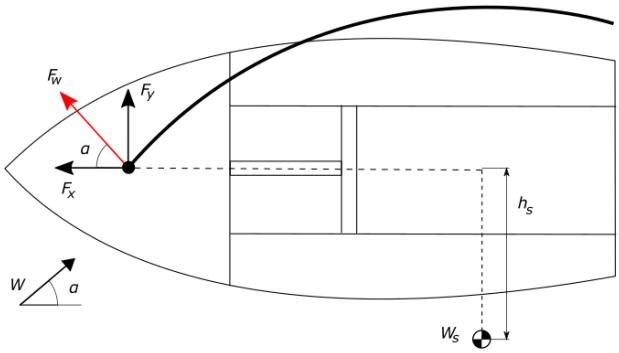

Figure 27: front view of the sailor position and sail centre of pressure.

The values from *Figure 26* and *Figure 28* are:

X	Value
W	10 knots[1]
α_w	30°
w_s	80 kg
h_s	1,848 m
h_w	0,900 m

Table 9: values from the previous figures.

From here, we can obtain the lateral wind force using equilibrium of moments:

$$F_y \cdot h_w = 9{,}81 \cdot W_s \cdot h_s \rightarrow F_y = 382{,}208\ N$$

Simple trigonometry will give us the value of the longitudinal force:

$$F_x = \tan \propto_w \cdot F_y \rightarrow F_x = 220{,}668\ N$$

And finally we obtain the moment generated by the wind:

$$M_w = h_w \cdot F_x \rightarrow M_w = 407{,}794\ Nm$$

[1] As mentioned in *chapter 3.1.2,* 10 knots correspond to a moderate wind intensity. In addition, the value of α indicates that the dinghy is sailing beam reach.

Now we have all the forces involved under foiling conditions but for the moments generated by the hydrofoils themselves, M_1 and M_2. It has been decided to neglect them since their magnitude will be significantly inferior to M_w.

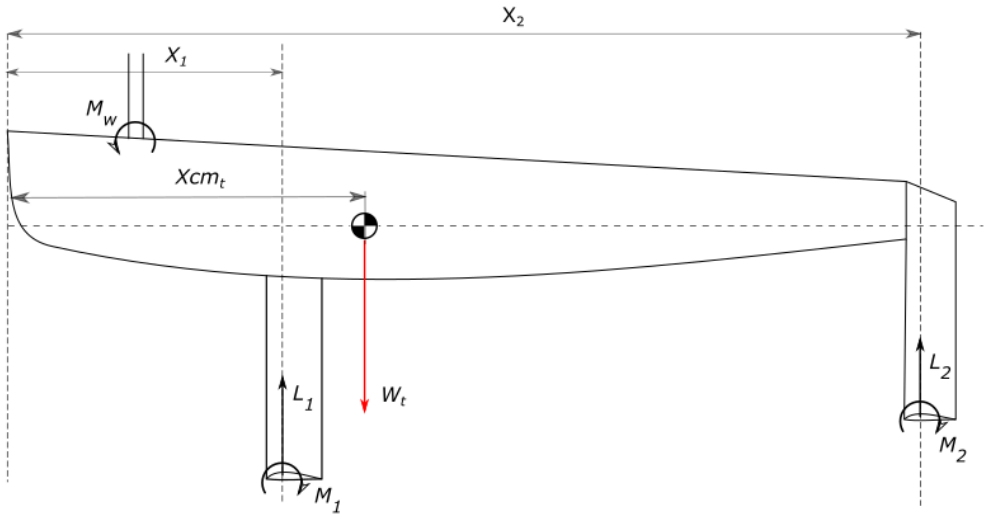

Figure 29: forces involved during stable flight.

Using *Equations (15)* and *(16)* we finally obtain the lifts to be generated by both hydrofoils:

$$L_2 + L_1 + (w_t{}^2) \cdot 9{,}81 = 0 \qquad (19)$$

$$M_w + L_2 \cdot (X_2 - Xcm_t) - L_1 \cdot (Xcm_t - X_1) = 0 \qquad (20)$$

Combining the previous equations we are left with an equation system which has the following solutions:

$$\mathbf{L_1 = 1.116{,}20\ N}$$

$$\mathbf{L_2 = 265{,}47\ N}$$

Therefore, with these values in mind, it can be said that the front foil needs to generate 80% of the total lift, while the rear foil accounts for the other 20%.

[2] W_t corresponds to the sum of the weight of all the components plus the sailor's body mass. It has been considered that the centreboard foil and rudder foil will weigh the same as the centreboard and rudder, respectively.

4.4.2.2. Surface calculation

Now that we know the forces that the foiling surfaces have to generate and the speed and medium in which they have to operate, using the explained wing theory we will determine the surface dimensions.

We have previously analysed the bi-dimensional profile NACA 63-412 on XFLR5 under the stable flight conditions, obtaining its C_l curve, (Figure 15) the linear section of which has a slope $C_{l\alpha} = 0{,}1145$. However, the centreboard foil when taking off will have a fully deflected flap, and therefore we must also determine the C_l of the flapped foil. The addition of the flap does not modify the slope of the linear segment but changes the intersection point with the x-axis since it displaces the curve to the left, improving the stall behaviour.

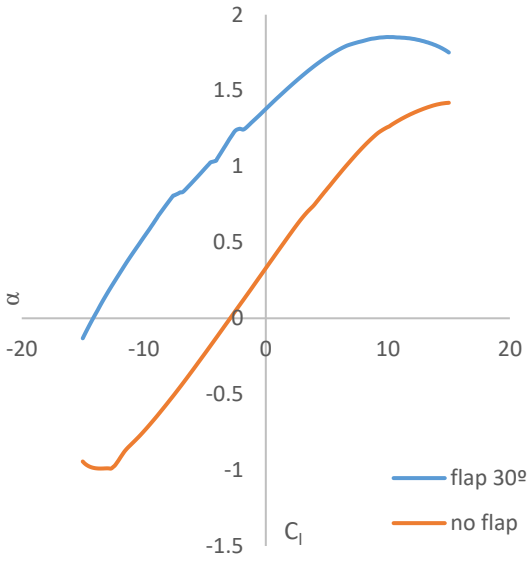

Figure 30: comparison between the flapped foil and the normal foil.

We have previously decided on an intrinsic angle for both hydrofoils of 1° since at this angle they less drag is generated. From *Figure 30* we can see that at 1° the foil with a 30° flap more than triples the lift generated by the foil without flap (1,456>0,350). The linear section of the represented C_l can be expressed as *eq.(6)* indicates:

$$30° \text{ flap} \rightarrow C_l = 0{,}097\alpha + 1{,}387 \quad (21)$$

$$\text{no flap} \rightarrow C_l = 0{,}1145\alpha + 0{,}337 \quad (22)$$

We can observe that as explained, the slopes are nearly equal and the flap curve is displaced to the left ($0{,}0970 \cong 0{,}1145$).

The three-dimensional C_L curve is expressed also as $\mathrm{C_L} = \mathrm{C_{L\alpha}} \cdot \alpha + \mathrm{C_{L\alpha 0}}$. Combining it with *eq.(8)* & *eq.(10)*, the expression expands to:

$$\frac{\mathrm{L}}{\frac{1}{2}\rho \mathrm{u}^2 \mathrm{S}} = \frac{\mathrm{C_{l\alpha}}}{\left(1 + \frac{\mathrm{C_{l\alpha}}}{\pi \Lambda}\right)} \mathrm{e} \cdot \alpha + \mathrm{C_{L\alpha 0}} \qquad (23)$$

From which we know all the variables but for the surface ($\Lambda = \mathrm{b}^2/\mathrm{S}$), $\mathrm{C_{L\alpha 0}}$, and b. A low **Oswald factor** e of 0,7 has been chosen to ensure that the obtained surface meets the requirements, and the **angle of attack** will be the hydrofoils intrinsic angle of 1°. A **span** of 1,2 m will be considered for the centreboard foil, and 0,82 m for the rudder foil.

Thus, a second equation must be defined if an exact solution must be extracted.

It is known that both the bi-dimensional plot and the three-dimensional approximation intersect the y-axis at the same point, denominated p ($\mathrm{p_f}$ when studying the flap configuration).

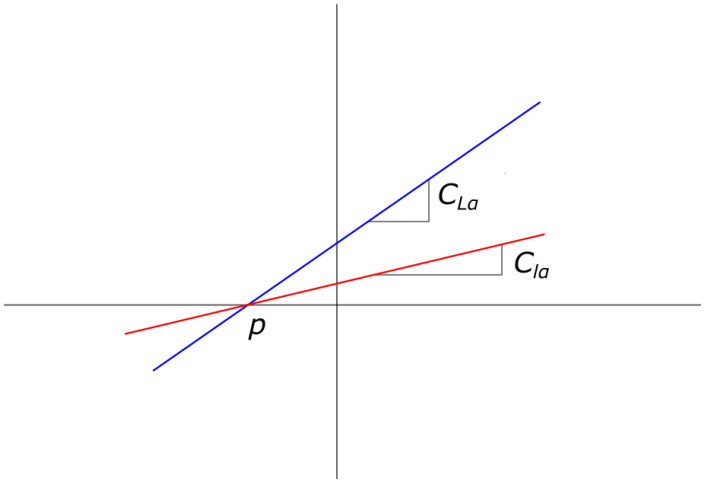

Figure 31: intersection between the bidimensional and tridimensional C_l plots.

Therefore, we obtain the following expression:

$$\mathrm{C_{l\alpha}} \cdot \mathrm{p} + \mathrm{C_{l\alpha 0}} = \frac{\mathrm{C_{l\alpha}}}{\left(1 + \frac{\mathrm{C_{l\alpha}}}{\pi \Lambda}\right)} \mathrm{e} \cdot \mathrm{p} + \mathrm{C_{L\alpha 0}} \qquad (24)$$

a) Centreboard hydrofoil surface

To obtain the surface of the centreboard flap, we will consider taking off conditions, which as mentioned above involve a speed of 2,8 m/s and a 30° deflected flap. In addition, we will use seawater density of 1.024 kg/m^3 and consider the lift obtained on previous calculations of 1.116,2 N. Combining equations *(21)*, *(23)* & *(24)* we obtain:

$$0{,}097 \cdot \left(p_f + \frac{0{,}7}{\left(1 + \frac{0{,}097 \cdot S_c}{\pi}\right)} \right) + C_{L\alpha 0} + 1{,}387 = 0 \qquad (25)$$

$$\frac{0{,}097}{\left(1 + \frac{0{,}097 \cdot S_c}{\pi \cdot 1{,}2}\right)} 0{,}7 + C_{L\alpha 0} - \frac{1.116{,}2}{\frac{1}{2} 1.024 \cdot 2{,}8^2 \cdot S_c} = 0 \qquad (26)$$

From here, we can determine the surface of the centreboard hydrofoil $\mathbf{S_c = 0{,}24\ m^2}$, knowing that $p_f = -14{,}2$.

b) Rudder hydrofoil surface

The dimensions of the rudder hydrofoil are related to the cruise conditions and not the take-off conditions. Therefore, when taking off it will be producing less lift than necessary to ensure flight if the angle of attack is not modified. Luckily, due to the foil double foil distribution, when taking off the centreboard foil will tilt the hull backwards, increasing the angle of attack of the rudder foil.

Firstly, we must know the **cruise speed**. At this speed, the **centreboard** hydrofoil must be able to maintain flight with the flap deflected 0°. We can compute the speed for different surfaces at which the centreboard produces the 1.116,2 N. This can be represented on a graph where we can determine the speed at which the necessary lift is achieved with the previously obtained surface.

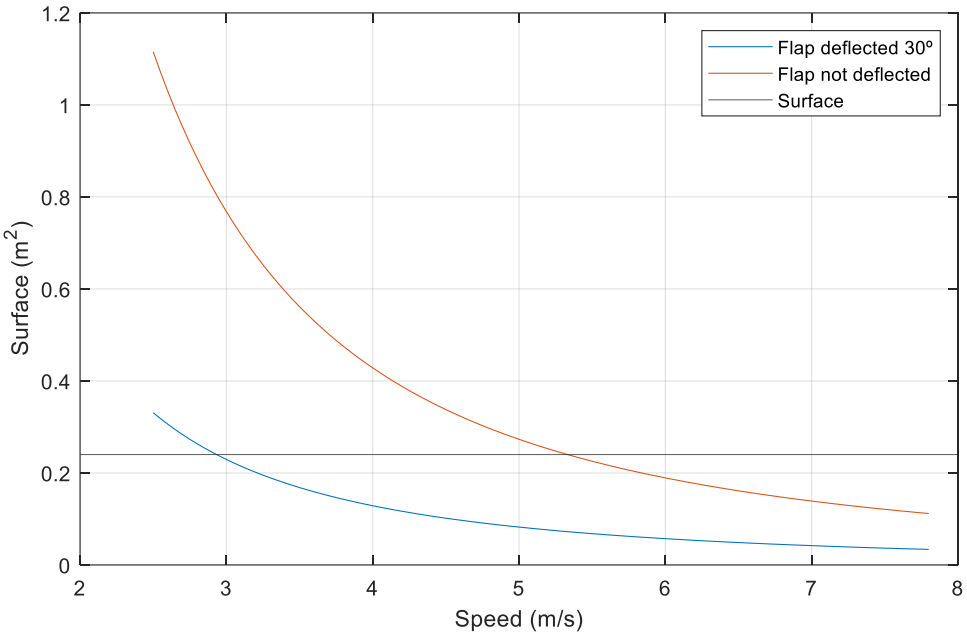

Figure 32: surface-speed plot for the centreboard hydrofoil.

We obtain a **cruise speed of 5,4 m/s.**

For this speed, we repeat the procedure followed for the centreboard hydrofoil but using *eq.(22)*, a lift of 265,47 N and considering the span of 0,82 m to obtain the rudder hydrofoil results.

$$0{,}1145 \cdot \left(p + \frac{0{,}7}{\left(1 + \frac{0{,}1145 \cdot S_r}{\pi}\right)} \right) + C_{L\alpha 0} + 0{,}337 = 0 \qquad (27)$$

$$\frac{0{,}1145}{\left(1 + \frac{0{,}1145 \cdot S_r}{\pi \cdot 0{,}82}\right)} 0{,}7 + C_{L\alpha 0} - \frac{265{,}47}{\frac{1}{2} 1.024 \cdot 2{,}8^2 \cdot S_r} = 0 \qquad (28)$$

Knowing that $p = -2{,}9$, we obtain the rudder foil surface, $\mathbf{S_r = 0{,}09\ m^2}$

4.5. Centreboard hydrofoil

Once the foil's surface has been determined and knowing that it must incorporate a 30% of the chord flap and present a tapered platform, now we can define its dimensions.

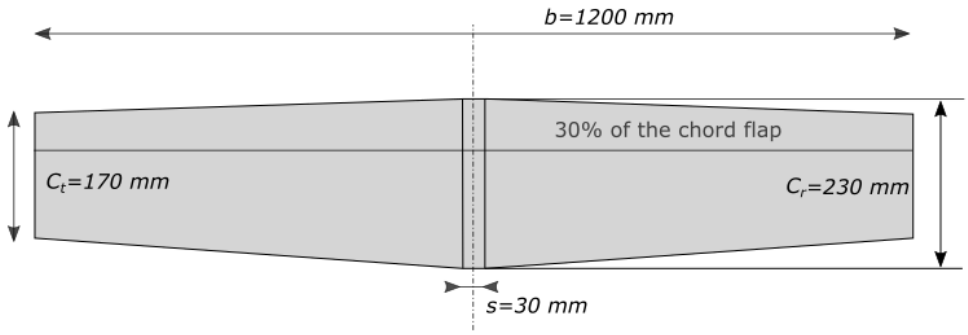

Figure 33: centreboard foil hydrodynamic dimensions.

We can see the centre of the foil, denominated section s, has been made of a constant chord to serve as a surface to connect the vertical strut. The dimensions of the root chord and the tip chord are 230 mm and 170 mm respectively. The tip has an offset of 42 mm so the trailing edge of the contact point between the flap and foil is completely horizontal.

The architecture will not present a dihedral angle nor twist to simplify the construction process. Furthermore, dihedral angles on hydrofoil configurations might have an undesirable behaviour since the tips of the foil will be closer to the surface and thus lose performance.

4.5.1. Centreboard strut

The centreboard foil will be attached to a vertical strut with a symmetrical NACA 0012 profile. At the same time, the strut will be fixed to the centreboard hole of the Europe's hull.

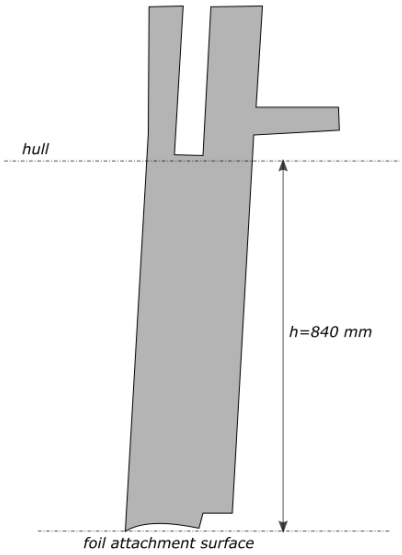

Figure 34: centreboard strut hydrodynamic dimensions.

The dimensions of the strut have been chosen considering a flight height of 0,4 m and the submergence factor influence. At the chosen flight height the proximity to the surface of the foil should be sufficient so that the submergence factor does not have an impact on the generated lift. The geometry of the strut will be discussed further below in *chapter 5.2.2.*

The NACA 0012 is a symmetrical profile. This means that it will not be generating any lateral forces. From all the other symmetrical NACA series we have elected this profile mainly for its thickness; a thicker profile is less likely to suffer from structural fatigue. In addition, thicker profiles are easier to manufacture.

4.6. Rudder hydrofoil

The dimensions of the rudder hydrofoil are the following:

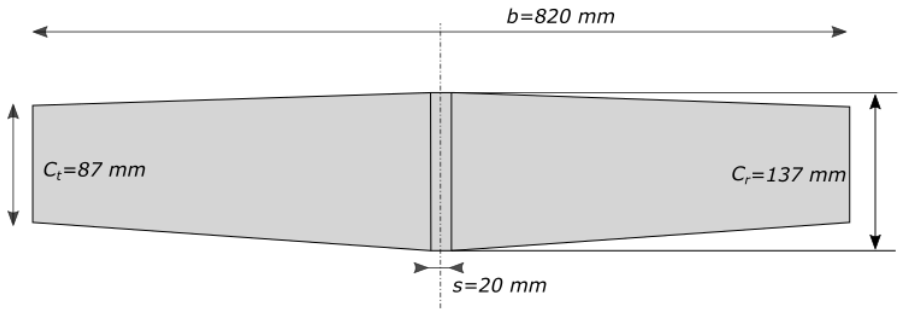

Figure 35: rudder foil hydrodynamic dimensions.

Again, section s has been added to provide additional surface to attach the vertical strut. Also, the foil will not present dihedral angle nor twist due to mentioned reasons.

4.6.1. Rudder strut

The rudder foil will be attached to a vertical strut of also a symmetrical NACA 0012 profile. This strut will also act as a rudder and its dimensions have been defined considering the flight height and trying to minimise the submerge factor as much as possible when stable flight is achieved at 0,4 m.

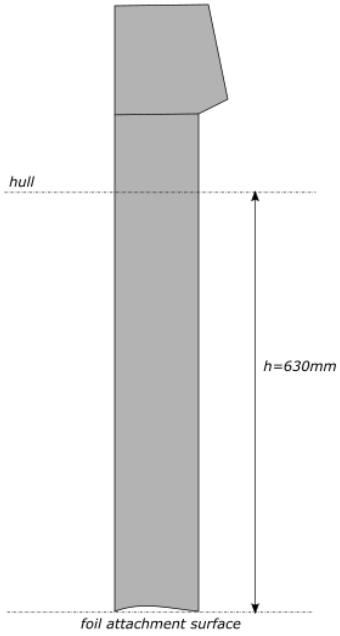

Figure 36: rudder strut hydrodynamic dimensions.

4.7. Hydrodynamic and stability analysis

Once all the foil geometries have been defined, we can introduce them to the XLFR5 software to analyse its hydrodynamic performance and stability. We will test the configuration during cruise speed or 5,4 m/s. Therefore, the flap of the centreboard foil must be deflected 0°. Since the struts have not been completely defined and the drag of the Europe's hull is not known we cannot obtain valid results of the total drag force of the configuration. In other words, we can only validate if the configuration achieves sufficient lift and stability at cruise speed.

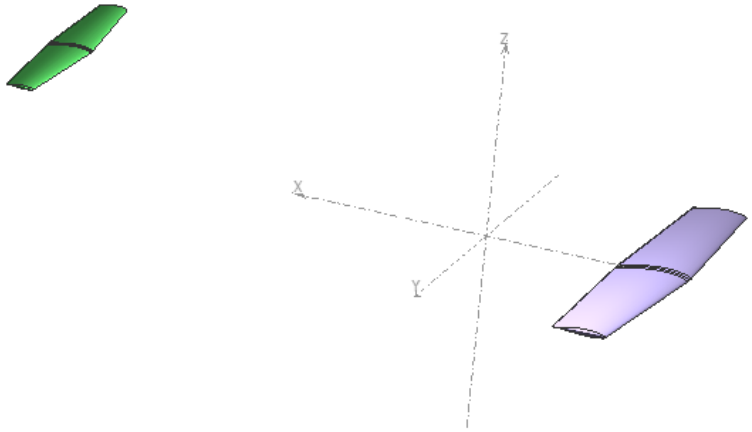

Figure 37: representation of the hydrofoils on XFLR5.

Firstly, the forces and moments acting over the dinghy as well as the foil distribution have to be computed on the software. Then, an analysis is defined with the cruise conditions. The following plots were obtained:

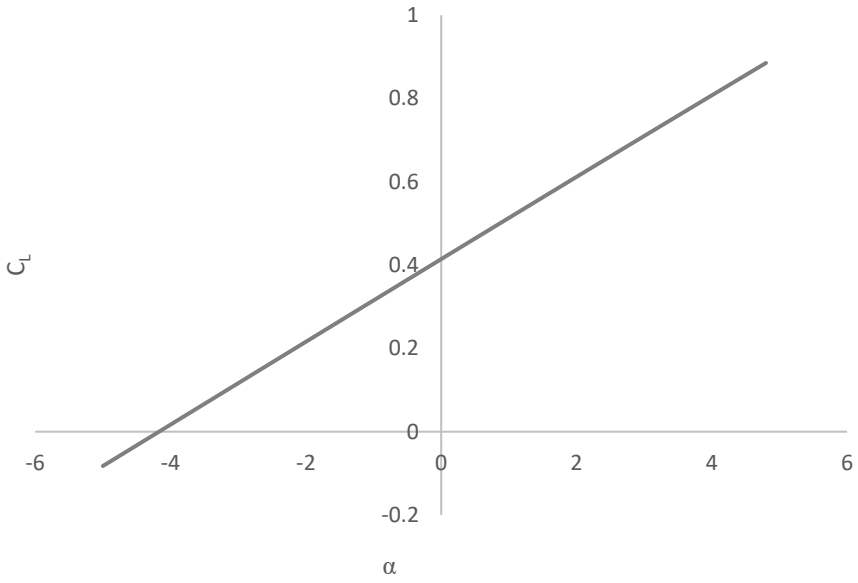

Figure 38: C_L of the configuration.

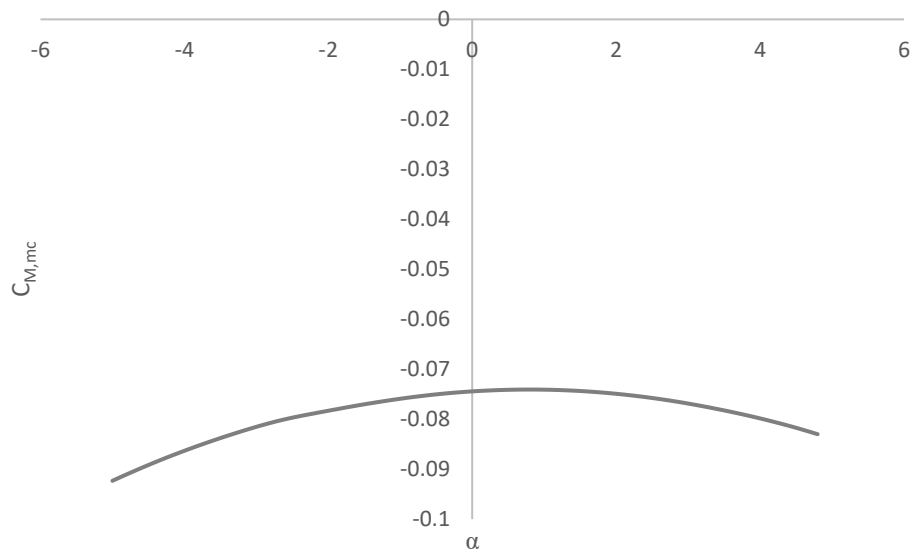

Figure 39: $C_{M,mc}$ of the configuration.

During cruise conditions, the foil's angle of attack should be the intrinsic angle of attack of 1°, already considered in the defined geometry. Therefore, we have to study the parameters at a null angle of attack.

Figure 38 indicates that for a 0° angle of attack, speed of 5,4 m/s and null flap deflection of the centreboard foil flap, the foils generate a total lift of 1.490 N. Therefore, the configuration under cruising conditions generates 108% of the needed force, communicating the correctness of the previous mathematical development.

The results of *Figure 39* are slightly concerning and indicate that the configuration is not stable, at least for negative angles of attack. Moreover, the equilibrium point is not found at 0°, indicating a deviation between the obtained results on chapter and the simulation. This could be attributed to the non-inclusion of the aerodynamic moments on the sizing calculations. However, these negative results could be rectified by moving the position of the sailor forwards 10 cm. The analysis is repeated with the modified centre of gravity, obtaining the following plot:

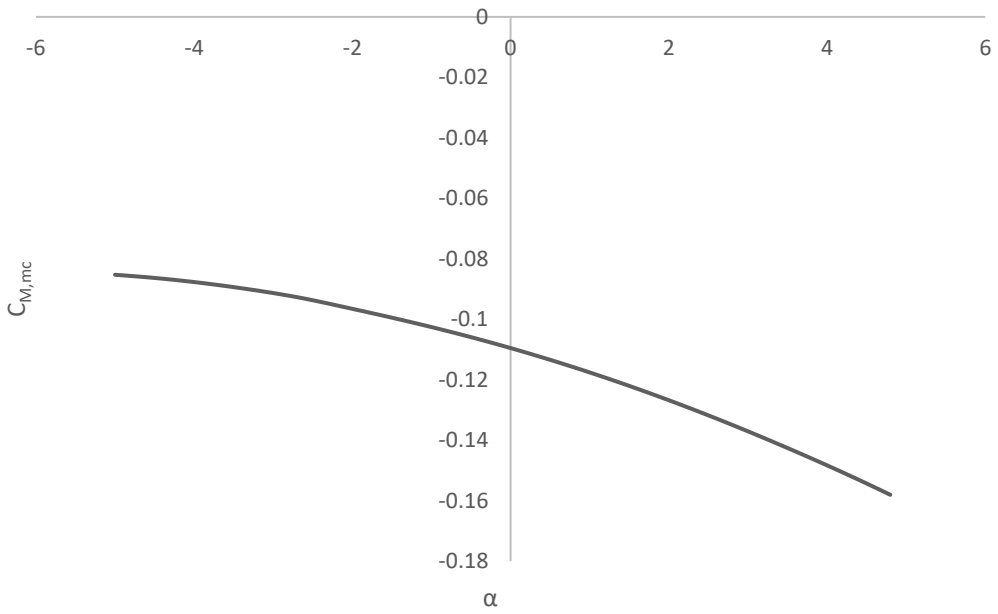

Figure 40: $C_{M,mc}$ of the modified configuration.

By moving the sailor's position, the configuration has become stable. Now, if the configuration's angle of attack increases due to a perturbation the additional generated moments will mitigate it. Still, the equilibrium point is located at approximately -6°. This means that under cruise conditions the sailor would need to constantly adjust its position to maintain the null angle of attack since at 0° the configuration tends to decrease the angle of attack. Consequently, we can conclude that the sized foils fulfil the requirements of lift generation and stability but might require constant imputes from the sailor to avoid pitching of the hull under cruise conditions.

5. FINAL DESIGN

In this section, the development of all the components will be discussed. A list of all the elements of the assembly and classification can be found in *ANNEX A.*

5.1. Control mechanism

The control mechanism is responsible for the adjustment of the centreboard flap. It must be able to measure the ride height and modify the flap deflection accordingly. The WASZP and MOTH use a mechanical system that is directly connected to the flap. This mechanism consists of a wand hanging out of the hull with the tip floating over the surface. Changes in the ride height will rotate the wand, and through a lever system, the flap position is instantly adjusted. The system itself it's not complex at all, but it consists of many mechanical pieces which can be difficult to manufacture. Furthermore, the trim of the wand and lever system might consist of trial and error hand adjustments.

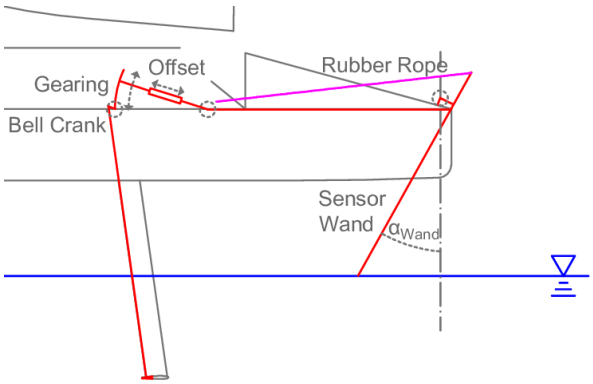

Figure 41: MOTH control mechanism. [15]

Instead of the lever system connecting the wand to the flap, a PID controller can be used. The advantages of an electrical system are the reduced number of pieces and the possibility of performing precise adjustments of the system response. However, it requires a power supply and all the electrical components must be strictly protected from water. Moreover, the design of a precise PID is a complex task out of the scope of this project.

Therefore, it has been decided to use a mechanical control system similar to the ones found on the MOTH or the WASZP.

5.1.1. Wand position

The MOTH and WASZP have the wand located at the bow of the hull. This position allows the wand to sense variations in the hull's pitch before the ride height is modified. This characteristic allows a smoother ride since the control system anticipates the height variations. The disadvantages of this configuration are the need to install support at the bow hull for the wand as well as a more complex connection system between the flap and the wand, like in *Figure 41.*

An alternative is to install the wand on the centreboard strut. The response of this configuration is not as smooth as the bow wand but it can be installed without modifying the hull of the dinghy. Also, it requires a simpler connection system between the flap and the wand.

Since installing support at the bow of Europe's hull can be a difficult task due to the lack of fixing points, it has been decided to install the sensing wand at the centreboard strut.

5.1.2. Mechanism concept

As previously announced, the wand has to sense the height of the ride, hence a **floating device** must be attached at its tip. The wand is made of a 500 mm carbon fibre tube. At the other end, the wand is attached to a **lever** installed at support fixed on the centreboard strut. This lever rotates when the ride height varies, pushing the **main rod**. When the main rod moves upward or downwards, a **seesaw** bascules over the **centreboard plate**, transmitting the movement to the **flap rod**. This last element is directly connected to the **flap** and modifies its deflection.

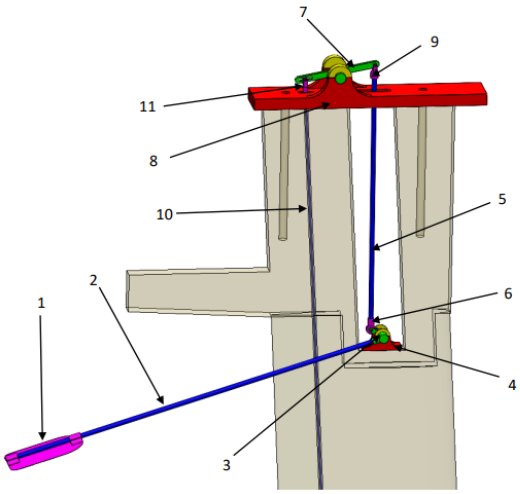

Figure 42: upper control mechanism components.

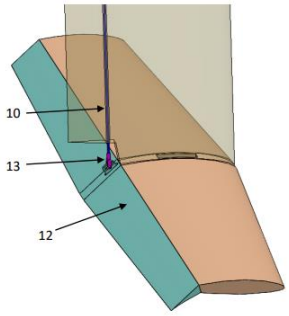

Figure 43: lower control mechanism components.

Element	Number
Floating device	1
Wand	2
Lever	3
Lever support	4
Main rod	5
Main rod-lever connector	6
Seesaw	7
Centreboard plate	8
Main rod-see saw connector	9
Flap rod	10
Flap rod-see saw connector	11
Flap	12
Flap rod-flap connector	13

Table 10: control mechanism components.

5.1.3. Flap trim

The control system has to be trimmed appropriately to deflect the flap properly and allow a constant height and stable flight. Previously it has been explained that to take off the flap must be deflected 30°. Once the cruise speed and height are achieved, the flap deflection must be null. As the dinghy increases its speed, the foiling surfaces will generate more lift, and the ride height will also increase. Therefore, the flap must also provide negative deflections to reduce the lift when necessary, since a ride too close to the surface can compromise the foil's functionality (*Figure 11*). The designed control mechanism provides the following wand and flap deflections for the defined ride heights:

Ride height h_r [mm]	Wand deflection α_w [°]	Flap deflection α_f [°]
0-190	20	30
410	54	0
480	72	-10

Table 11: flap deflection for different ride heights.

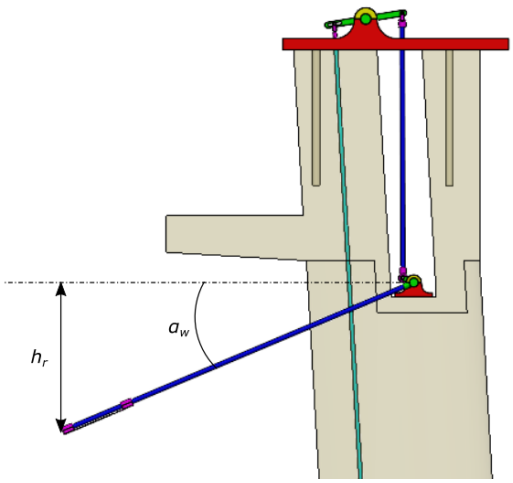

Figure 45: wand deflection and ride height.

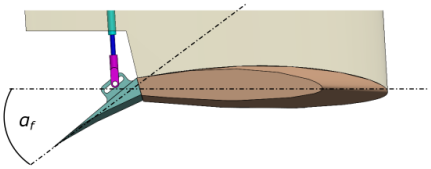

Figure 44: flap deflection.

Considering a linear behaviour, we can express the control mechanism actuation with the following plot:

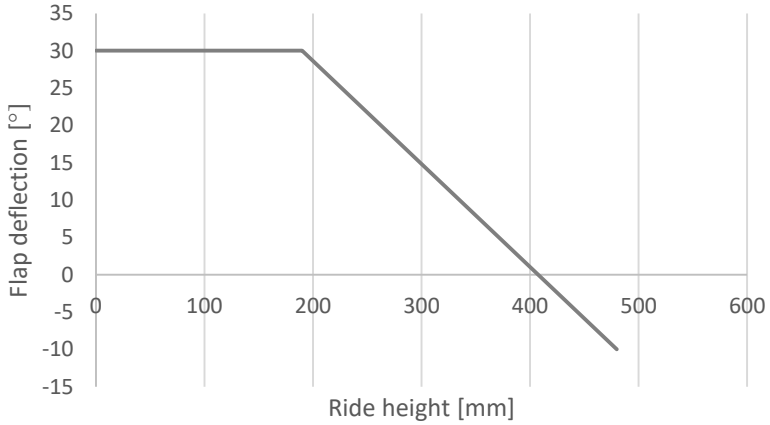

Figure 46: flap deflection vs ride height plot.

We can see that the designed control mechanism behaves as expected and should provide a stable ride at a constant height of 410 mm.

5.2. Centreboard assembly

5.2.1. Centreboard foil and flap

The geometry of the foiling surface was previously defined in a rigorous mathematical sizing and tested using XFLR5. A hole at the centre of the foil has been added to permanently fix the centreboard strut.

On the other hand, the flap has been sectioned from the foil model and will be designed as a completely different piece. The geometry of both foil's trailing edge and flap have been adapted to allow the needed deflections. Moreover, the flap includes a support for a slat mechanism to connect it with the defined control system.

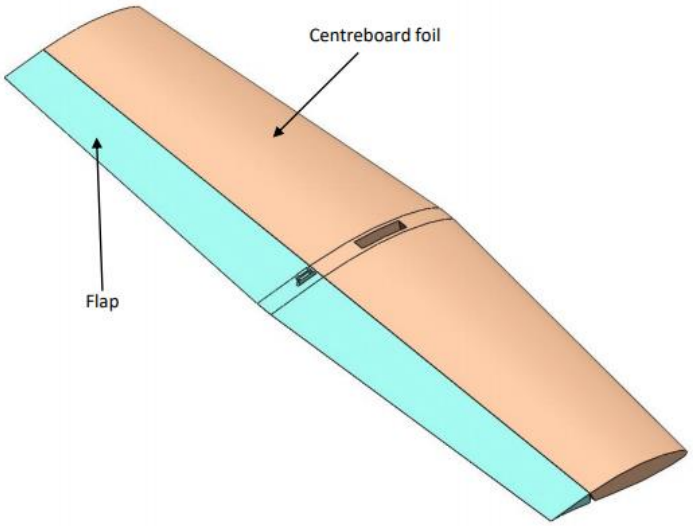

Figure 47: centreboard foil and flap CAD model.

The will be attached to the foil by means of four nylon hinges.

5.2.2. Centreboard strut

The strut geometry was designed considering the dimensions of the hull's centreboard hole and the defined ride height. At the bottom surface, an extrusion has been included to fit into the mentioned foil hole. This fixation is meant to be permanent and would require the addition of an adhesive such as epoxy resin.

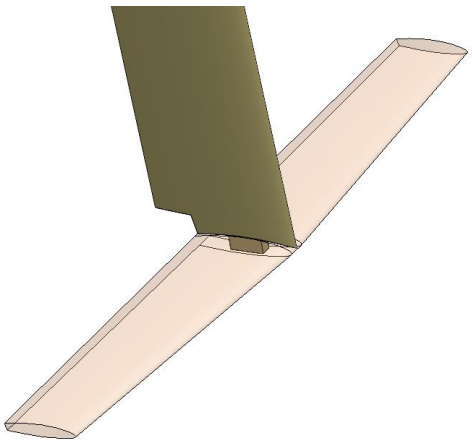

Figure 48: centreboard strut and foil attachment.

On the other hand, to fix the strut to the Europe's hull two stoppers have been modelled. These pieces will prevent the strut from slipping upwards when the lifting force is applied and will also be glued with epoxy resin directly to the strut.

The centreboard strut- foil assembly will be introduced to the hull's centreboard hole from the bottom surface. To prevent it from falling, two M10 threaded rods of 230 mm will be inserted and fixed with adhesive into the strut. Then, using M10 nuts and washers the strut will be secured to the centreboard plate, preventing the movement of the assembly. This fixation is removable and fulfils the project technical requirements. Since this fixation is not permanent the foil can be installed and removed without damaging the hull. Further details of all the fixing elements can be seen in *ANNEX A.*

The geometry has suffered slight modifications to accommodate the control mechanism. Most noticeably, a capillary tube of 1.120 mm, with an internal diameter of 4 mm and an external diameter of 5 mm, runs across the strut. The flap rod is supposed to fit inside it.

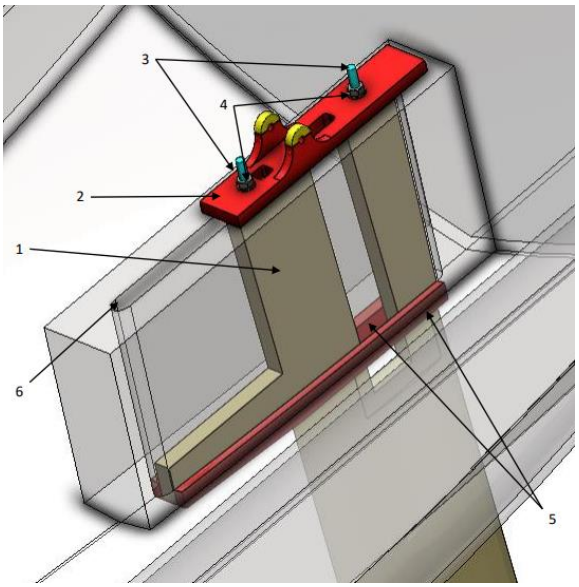

Figure 49: centreboard strut and its fixing elements.

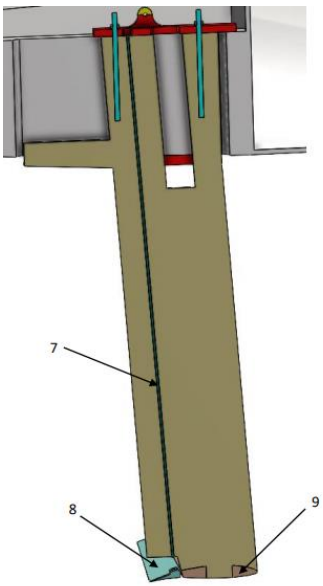

Figure 50: capillary tube inside the centreboard strut.

Element	Number
Strut	1
Centreboard plate	2
M10 threaded rods	3
M10 nuts and washers	4
Stoppers	5
Hull's centreboard hole	6
Capillary tube	7
Flap	8
Centreboard foil	9

Figure 51: centreboard strut and its fixing elements.

5.3. Rudder assembly

5.3.1. Rudder foil

The geometry of the rudder foiling surface has been modelled in the same manner as the centreboard counterpart. Also, hole has been added to serve as a fixing point for the rudder strut.

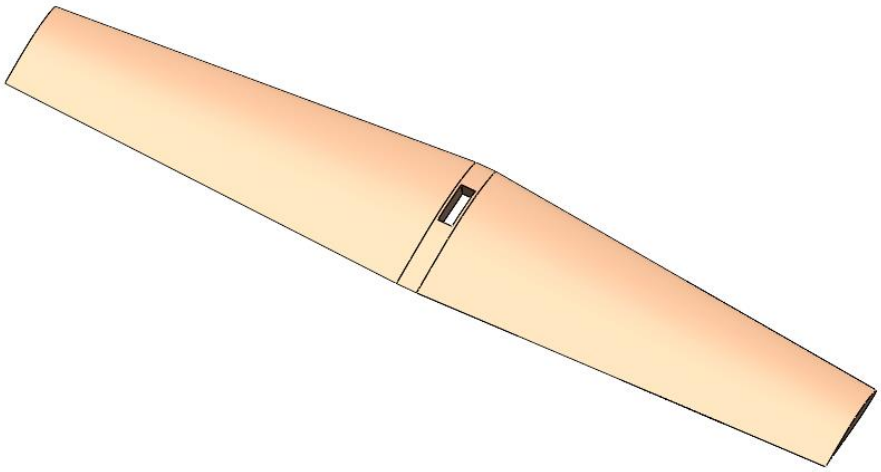

Figure 52: rudder foil CAD model.

5.3.2. Rudder strut

The rudder strut has been designed with a fixed angle of attack. It must fit the regulatory Europe's rudder stock and be completely removable. At the bottom surface, like in the centreboard strut, an extrusion has been added to fit into the rudder foil hole. The union between the rudder strut and foil is also meant to be non-removable and needs the application of an adhesive such as epoxy resin. Since instead of the rudder we are attaching the rudder strut, this last element must also pivot to allow the steering of the dinghy.

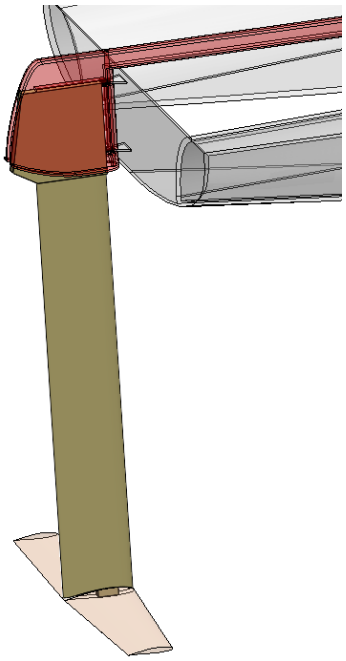

Figure 53: rudder strut and foil assembly installed to the rudder stock (red).

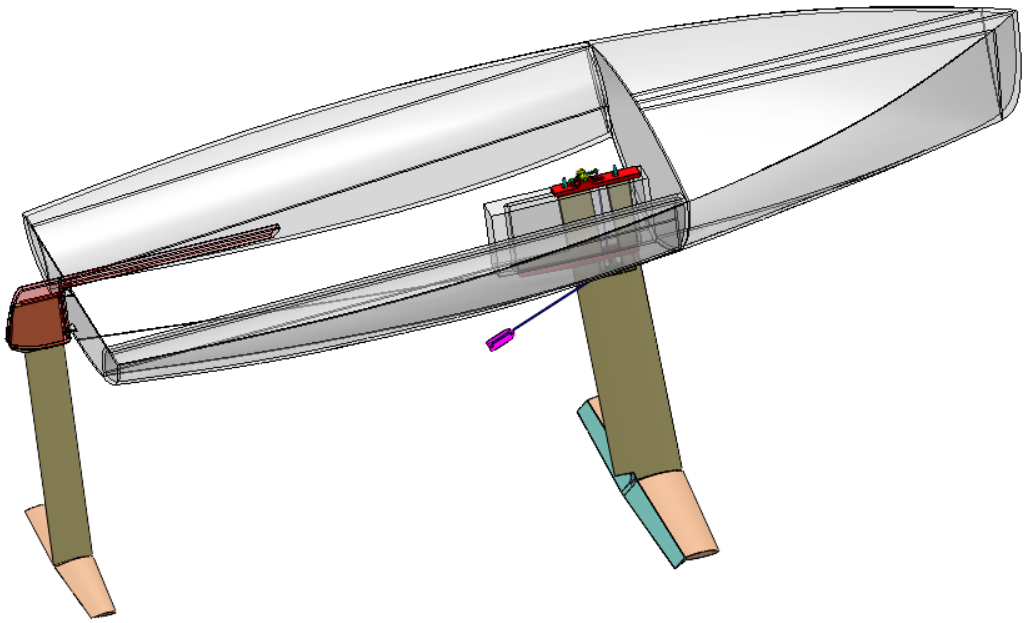

Figure 54: global assembly.

5.4. Material selection

Once the concept has been defined, the materials in which the elements have to be listed. The said components can be divided into four categories: fixing elements, secondary parts, main bodies and rods. The only components that have to be manufactured are the secondary parts and the main bodies. The rest can be directly purchased. Its price is specified in the *BUDGET* document.

5.4.1. Main bodies

The main bodies category includes the lifting surfaces and struts. Their function is to generate the lifting forces and transmit them to the hull. Therefore, they must withstand major loads. In addition to that, they must be lightweight and waterproof, since they have to be easily lifted and operate underwater. In the dinghy industry, similar components such as the rudder or centreboard are manufactured using composites. Therefore, it is interesting to use **composite materials** for the main bodies due to their exceptional mechanical properties, relative lightness and ease of moulding.

To speed up the manufacturing process a monocoque construction has been chosen for the main bodies. This means that there will not be any internal structure and the composite skin will distribute and support the structural loads by itself. The election of the composite and further details of the manufacturing process can be seen in chapter 6.

5.4.2. Secondary parts

The secondary parts category includes multiple customised mechanical and structural components which must be prototyped. The majority of these components do not withstand critical loads and therefore faster and cheaper prototyping methodologies can be used. It has been decided that all of these components will be 3D printed.

The most popular 3D printing materials for basic 3D printers are PLA, ABS and nylon. All of them can be bought for a reasonable price but present different properties.

- **PLA**

PLA or Polylactic Acid is the default filament of choice for most extrusion-based 3D printers. The main advantages of this material are its low melting temperature which allows the printer to operate at lower temperatures, increasing the lifespan of certain components. PLA is also known for its stiffness and good overall strength and it can be considered biodegradable since is derived mainly from corn corps or sugar. However, it is the less durable of the three materials and also the densest, and it presents the lowest service temperature.

- **ABS**

ABS or Acrylonitrile Butadiene Styrene was one of the first plastics to be used in additive manufacturing. ABS is known for its toughness and impact resistance and therefore the resulting pieces are less susceptible to wear than if they were made of other materials. It also presents a higher melting point, making it more difficult to work with than PLA, but the resulting elements can withstand harsher conditions. One of the main downsides of this material is its heavy contraction process when cooling, making it difficult to work with.

- **Nylon**

Nylon, also known as Polyamide, is the only material of the three with partial flexibility. It presents a high impact resistance. However, Nylon is hygroscopic, which means that it absorbs moisture and water. Hence, it is not the ideal material for marine applications.

	PLA	**ABS**	**Nylon**
Ultimate strength	65	40	85
Stiffness	7,5/10	5/10	5/10
Durability	4/10	8/10	8/10
Maximum service temperature	52°C	98°C	95°C
Density	1,24 g/cm^3	1,04 g/cm^3	1,06 g/cm^3
Printability	9/10	8/10	8/10
Extruder temperature	190-220 °C	220-250 °C	220-270 °C
Bed temperature	45-60 °C	95-110 °C	70-90 °C
Biodegradable	Yes	No	No
Price/kg	20	30	40

Table 12: filament comparison.

Since the PLA is the only biodegradable alternative, it is less demanding to the 3D printer and presents more than adequate mechanical properties, it has been decided **that PLA will be the base material for all the secondary parts** and other 3D printing processes to be carried out.

6. PROTOTYPE MANUFACTURING

The objective of this project was initially to build a fully functional prototype. However, due to budget and schedule restrictions, the prototype has been scaled down to the centreboard foil and the flap, demonstrating that the manufacturing of such components is possible. Therefore, in the near future a fully functional prototype could be assembled, but for now, this is out of the scope of the project.

6.1. Flap

The flap, being a secondary part and a non-structural element, was 3D printed using PLA filaments as mentioned in *section 5.4.2.* Due to its complex geometry and being a non-structural element, it was decided to manufacture the flap with a 3D printer using PLA filaments. The used 3D printer, a Creality CR-10, can print within a space of 300x300x400 mm. It was not possible to print the whole flap section from one piece, and therefore it was divided into 5 sections which then would be assembled using adhesive and notches incorporated into the design. In addition, the edges have been rounded to increase the aesthetic appearance.

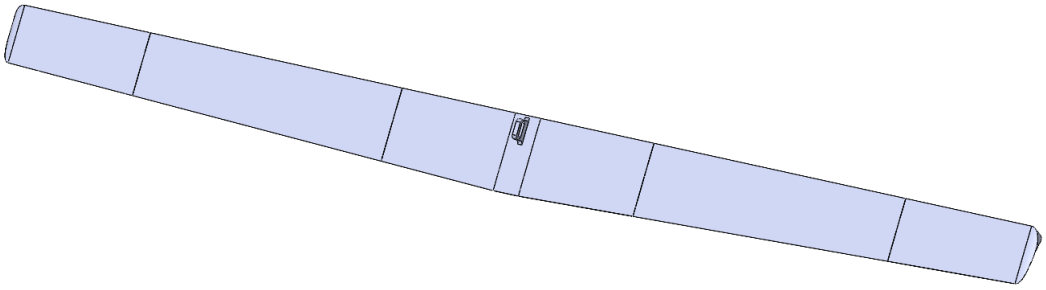

Figure 55: flap CAD model.

After conducting numerous tests, one of which involved the printing of a scale Europe dinghy hull, it was determined that the best parameters for printing the flap are a 10% infill and 3 exterior layers.

It is also very important to determine the tolerances for the notches. After conducting other several tests, it was determined that for the used nozzle of 0,4 mm, material (PLA) and finish quality, and the tolerance is 0,3 mm.

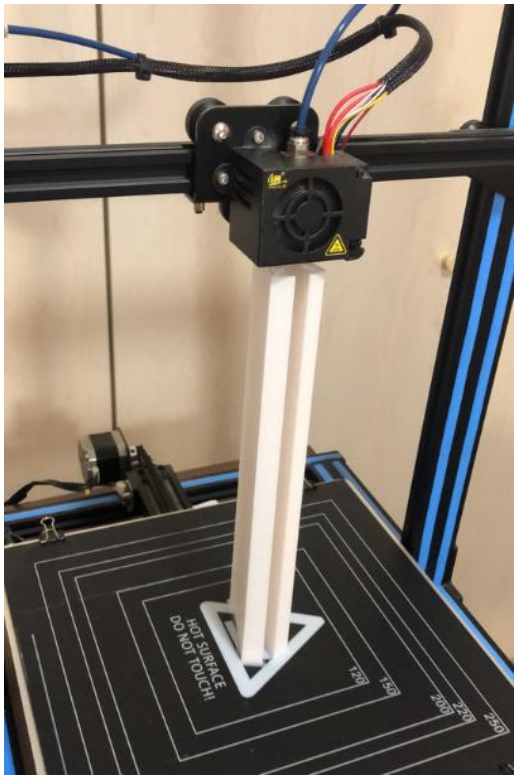

Figure 56: printing of the flap sections.

Figure 57: printed flap sections.

After the sections were printed, they were assembled and glued together using cyanoacrylate. The printer worked non-stop for 2 days and 3h, consuming a total of 360 g of PLA.

Figure 58: assembled flap.

6.2. Centreboard foil

The centreboard foil had to be manufactured using composite materials. Manufacturing composite processes usually involve some sort of moulding, to shape the matrix and reinforcement. Then, the material is cured, a process in which the reinforcement is fixed within the matrix. The curing process usually requires specialised machinery and the manipulation of composite fibres and after processes have to be done in an adequate environment with proper ventilation. For these reasons, it was decided to approach a specialised company in the sector.

Figure 59: N1Foils logo.

N1Foils is a company that specialised in the manufacturing of dinghy equipment, mainly centreboards and rudders, based in Cabrera de Mar. After an initial approach, the company manager Toni Riera offered its installations and expertise to develop the prototype.

6.2.1. Material choice

6.2.1.1. Reinforcement

N1Foils works with carbon fibre fabric and E-glass fibre fabric-based composites. Fibreglass and Carbon fibre have similar strength characteristics. Although fibreglass presents a slightly inferior tensile strength and stiffness, it is significantly cheaper, a key factor for the viability of the project. Therefore, it was decided to use fibreglass fabric as reinforcement. The used fabric is an E-glass woven twill, which is produced by the interlacing of warp (0°) and weft (90°) fibres. The fabric's integrity is maintained by the mechanical interlocking of the fibres.

6.2.1.2. Resin matrix

The resin of choice is Super Sap CLR double component Epoxy Resin. It presents a density of 1.170 kg/m^3 and the manufacturing company, Entropy Resins, claims that more than 40% of the resin mass comes from biologic products instead of petroleum. The main component of the Epoxy has to be mixed with the hardener at a volume proportion of 2:1.

6.2.1.3. Composite mechanical properties

A composite with a 65% fibre volume ratio of the said components presents the following mechanical properties:

Fibre volume ratio V_f [%]	65
Density ρ [g/cm^3]	1,83
Longitudinal modulus E_1 [GPa]	40,51
Transverse modulus E_2 (GPa]	13,96
In-plane shear modulus G_{12} [GPa]	3,10
Poisson's ratio ν_{12}	0,22
Longitudinal tensile strength X_t [MPa]	783,30
Transverse tensile strength Y_t [MPa]	64
Longitudinal compressive strength X_c [MPa]	298
Transverse compressive strength Y_c [MPa]	124
In-plane shear strength S_i [MPa]	69
Interlaminar shear strength S_{12} [MPa]	38

Table 13: mechanical properties of the composite to be manufactured.

6.2.1.4. Foam core

Following the philosophy of N1Foils, it was decided to use foam sheet as a core to avoid buckling of the glass fibre composite. The foam of choice is a PVC based foam provided by Gurit, with a density of 130 kg/m3. It presents a relatively soft surface that will easily adapt to the shape of the moulds. Its mechanical properties are the following:

Density ρ [g/cm^3]	0,13
Longitudinal modulus E_1 [GPa]	1,05
In-plane shear modulus G_{12} [GPa]	0,04
Poisson's ratio ν_{12}	0,37
Longitudinal tensile strength X_t [MPa]	18,80
Transverse tensile strength Y_t [MPa]	64
Longitudinal compressive strength X_c [MPa]	1,97

Table 14: mechanical properties of the foam of choice.

6.2.2. Mould manufacturing

The moulds had to be manufactured in the most cost-efficient manner. After some research, two possible alternatives were considered: CNC manufacturing or additive manufacturing using the available 3D printer. The CNC manufacturing process consists of carving the mould out of a solid piece of base material, usually wood, allowing for higher production speeds than additive manufacturing, as well as better finishes. However, no CNC machines were directly available and an external party had to be involved, dramatically increasing the price of the process. Therefore, it was decided to manufacture the moulds with PLA filament and the available printer. Although PLA is far less consistent than CNC wood and the process is relatively slow, some initial tests revealed that the material had sufficient strength and the surface finish was more than acceptable.

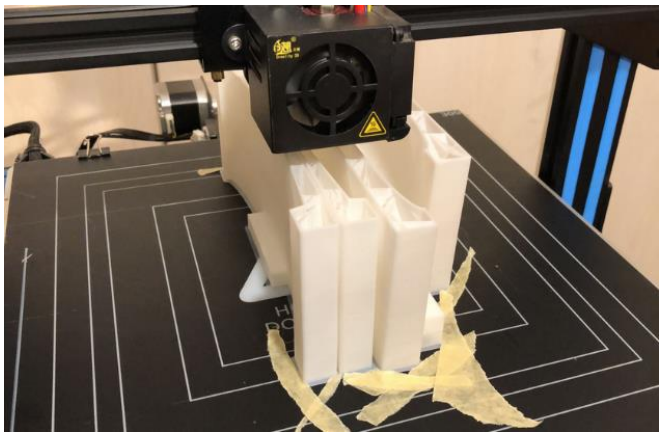

Figure 60: printing of the moulds.

The printing process was done with the minimum possible thickness which is 2 exterior layers, to reduce the waste of material, and an infill of 10%. Again, due to size limitations, the moulds had to be printed in sections and assembled afterwards using cyanoacrylate. In total, 3 printing sessions were carried out adding up to 154 h of printing and 1.235 g of PLA.

Figure 61: finished moulds.

Afterwards, the two resulting moulds were polished using 180 grit sandpaper for a smooth finish.

6.2.3. Composite manufacturing

Once the mould was made, the process of composite manufacturing could start. To begin, it was decided to use 2 layers of glass fibre fabric per face. Since the sole objective of manufacturing such a prototype is proving the validity of a construction method, it was decided to use as little material as possible. However, later a structural study will be conducted to see if the final result could withstand the calculated loads. All the necessary layers had to be cut from a glass fibre fabric role using a CNC machine with a circular blade head.

Figure 62: result of the CNC process.

Figure 63: CNC cutting the E-glass fibre fabric.

The same had to be done with the foam. The available foam sheet had a thickness of 12 mm. Therefore, it was decided to use two foam layers instead of one to produce the core. Afterwards, the resultant foam sheets had to be trimmed to a suitable shape using a polisher. Once the core fitted in between the two moulds, the composite manufacturing process began.

Figure 64: trimming of the foam core.

The followed process receives the name of hand lay-up. It consists of manually impregnating the fibres, fabric in our case, by directly applying the epoxy and impregnate the reinforcement with the help of a roller. The process began by adding a layer of glass fibre on top of the lower mould. The said mould was protected by a plastic sheet to prevent the epoxy from sticking to its surface.

Figure 65: hand lay-up process.

Figure 66: hand lay-up process over the foam core.

Then, another layer was added, followed by the two foam sheets which were also impregnated with epoxy. On top of that, the last two layers of glass fibre fabric were added. A total of 400 ml of epoxy and 200 ml of hardener were used. Then, the upper mould was attached on top of the composite sandwich (also protected by a plastic sheet) to close the assembly and pressure was applied over it using wood planks and three clamp screws. Finally, the result was left to cure for approximately 12 hours.

Figure 67: closed moulds.

Figure 68: closed moulds with applied pressure.

The following day, the moulds were removed. Due to the exerted high pressure, the moulds had cracked mainly on the leading edge.

Figure 70: deformities of the lower mould.

Figure 69: unfinished result after removing the moulds.

Further irregularities were produced by wrinkles on the plastic backs, which left marks over the surface of the foil. After some trimming and polishing, the final result came to light.

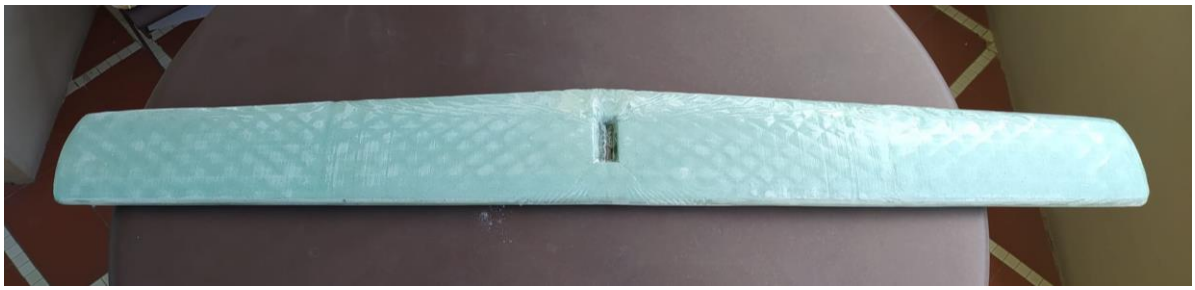

Figure 71: finished centreboard foil prototype.

Some of the imperfections had been scaled down, but still, the leading edge is far from the shape defined by the mould. However, with a more aggressive polishing process, the discrepancies could be rectified to obtain a more exact result.

6.2.4. Results and improvements

The final result of the centreboard foil manufacturing is a solid composite piece with a foam core and E-glass fibre reinforcement with some major irregularities mainly on the leading edge. As mentioned above, such irregularities were produced by the deformation of the moulds. If the moulds are printed with more infill or filled with epoxy resin, for example, they could increase their structural integrity and handle the pressures of the curing process. On the other hand, to prevent the epoxy from sticking to the mould's surface, plastic sheets were used. Such plastic sheets produced irregularities over the foil's surface. Therefore, a more refined alternative has to be studied and implemented.

Overall, it can be said that the manufacturing of foiling surfaces through the described method is feasible although it needs some improvements.

6.3. Centreboard foil structural study

The main objective of this subsection is to prove if the final result can withstand the calculated loads. SOLIDWORKS software was used for this purpose. The parameters of the materials had to be introduced and the composite sandwich was defined. Then, to simplify calculations, it was decided to use a constant lift distribution. This is not a realistic approach, since on a three-dimensional wing less lift is generated near the tips. A constant lift distribution means that more loads are generated. Therefore, if the material withstands the loads of the defined case, it means that it would also resist the real lift distribution.

A pressure was applied to the lower face of the foil, corresponding to the centreboard lift divided by the value of the same surface. $P = 1.116{,}20\ N/0{,}17\ m^2\ = \mathbf{6.764{,}84\ N/m^2}$.

The surface which is supposed to be connected to the strut was defined as a fix. Then, a mesh was defined and the simulation was run.

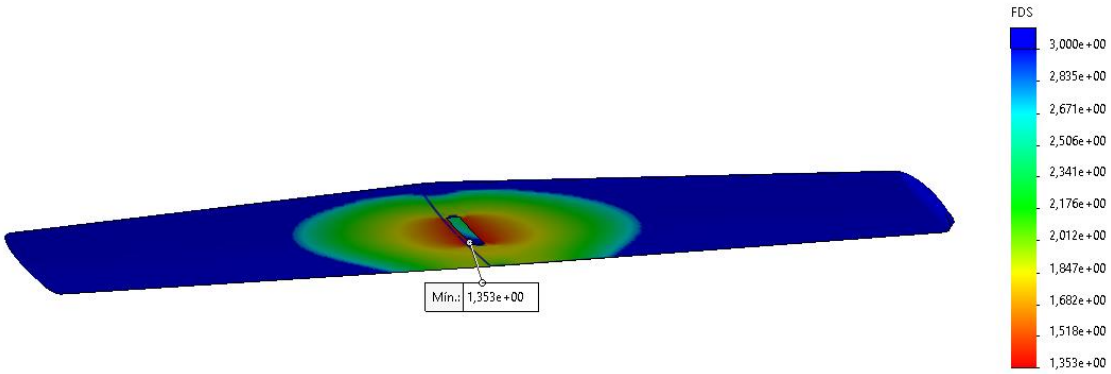

Figure 72: factor of safety at the lower surface of the foil & minimum value.

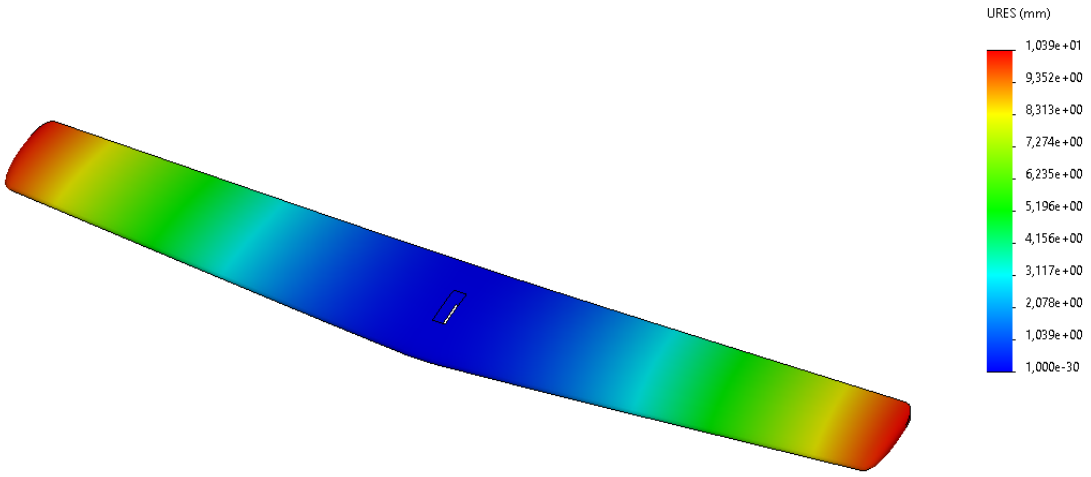

Figure 73: deformations under the defined loads.

The results show a minimum factor of safety at the centre of the lower surface of 1,353. The factor of safety is defined as:

$$\text{FoS} = \frac{\text{yeld stress}}{\text{working stress}} \tag{29}$$

Therefore, having a factor of safety superior to 1 means that the material is working below its limit. In our case, the foil can withstand 1,353 times the defined load before failure occurs. The deformation diagram also shows successful results, since the tips only flex a maximum of 10,39 mm. With these results on hand, it can clearly be said that the manufactured prototype can withstand the design loads.

7. BUDGET

The costs of manufacturing the fully functional prototype as well as of the whole project are specified in the *BUDGET* document. In this section, only the manufacturing costs of the flap and centreboard foil prototypes will be determined.

7.1. Additive manufacturing

As explained in *chapter 6*, the flap and mould of the centreboard foil were 3D printed. This process consumes PLA filament as well as energy in the form of electricity. Since we know the energy consumption of the used printer and the weight of the mentioned elements, we can approximate the total cost of the additive manufacturing process. One roll of PLA printing filament costs 20 € and weighs 1 kg, which gives us a relation of 0,02 €/g. On the other hand, the electricity cost is estimated to 0,276 €/kWh and the 3D printer consumes 0,7 kW. The cost of the machinery will not be considered since the used 3D printer was lent by a friend.

Additive manufacturing

	PLA [g]	Printing time [h]	Filament price [€/g]	Energy consumption [€/kWh]	Cost
Flap	360	51	0,02	0,276	17,05 €
Moulds	1.235	154			54,45 €
Total:	1.595	205			**71,5 €**

Table 15: additive manufacturing cost.

7.2. Composite manufacturing

The manufacturing costs of the centreboard foil were assumed by N1Foils. However, they will be determined to give the reader a broader picture of the project's cost. Moreover, the commute costs to the N1Foils workshop will also be considered.

Composite manufacturing

	Cost
3 h labour + machinery	100 €
0,7 m^2 of E-glass fibre fabric	10 €
0,4 m^3 of 2 cm thick PVC foam sheet	20 €
0,4 ml of epoxy + 0,2 ml of hardener	7 €
3 m plank of pine wood	27 €
Total:	**165 €**

Table 16: composite manufacturing cost.

A total of three car trips were done to the N1Foils workshop. The distance of the commute is 64 km and the used car consumes an average of 6,9 l/100 km of diesel, the cost of which is 1,24 €/l. All trips required paying a 1,28 € toll.

Displacements

Trips	Distance/trip [km/trip]	Fuel consumption [l/km]	Fuel price [€/l]	Toll [€/trip]	Cost
3	64	6,9/100	1,24	1,28	**20,27 €**

Table 17: displacements cost.

7.3. Total cost

The total cost of the manufactured prototype ascends to **256,77 €.**

Total

Additive manufacturing	71,5 €
Composite manufacturing	165 €
Displacements	20,27 €
Total cost	**256,77 €**

Table 18: total costs of the manufactured prototype.

8. ENVIRONMENTAL IMPACT

Although this is a project of relative minor dimensions in which no major manufacturing processes have been carried out, it is important to record and present the environmental impact of all the activities. The objective of this section is to give a general idea of how much of an impact can have little human activities such as this thesis and present possible solutions that could have made the project greener.

8.1. Direct impact

The main direct environmental impact of this project comes in the form of electricity consumption. The production of this thesis required the use of a desktop computer and the manufacturing of the prototype makes extensive use of a 3D printer. The total energy of the previous appliances has been estimated in the budget section.

Appliance	Working hours [h]	Energy consumption [kW]	Total energy consumption [kWh]
3D printing	100	0,7	70
Desktop computer	600	0,3	180
Table lamp	600	0,06	36
Total:			**286**

Table 19: energy consumption.

It is estimated that the Spanish peninsular electrical network emission factor is 0,27 kg CO2/kWh. Therefore, this project has led to the **generation of 77,22 kg of CO2.** Moreover, it is also interesting to determine the number of nuclear residues that this project generated. The values referring to the nuclear waste generation of the Spanish peninsular electrical network indicate that for every consumed kWh, 0,55 mg of nuclear waste are generated. Therefore this project **generated 157,3 mg of nuclear waste.**

To manufacture the centreboard prototype, a total of three car trips were done to the N1Foils workshop. The distance of the commute is 64 km. The used car consumes an average of 6,9 l/100 km of diesel and has CO2 emissions of 146 g/km. Therefore, those commutes supposed the emission of 28 kg of CO2, which add up to a **total of 105,22 kg.**

8.2. Indirect impact

All the materials involved in the manufacturing of the prototype have an impact on the environment. The raw materials for their products generally come from large industrial complexes and mining plants. Furthermore, their production requires a significate energy input which generally does not come from renewable energies. There is no way determining the impact that the production of the project's materials had on the environment, and thus it will not be quantified.

Luckily, the majority of the materials used, such as the PLA plastic and steel from the fixing elements and rods, can be easily recycled or processed once their lifespan is over. The same cannot be said about composite materials.

Composite materials are known for their exceptional mechanical properties and relative lightness. That is why they are used in the manufacturing of wind turbines and aircraft. However, the recycling of this material is a challenge of its own due to its heterogenic nature. There exist various technologies which can be used to recycle composites but generally it is an expensive process whose result presents an inferior quality to brand new composites.

Figure 74: wind turbine landfill. [16]

Proposing solutions for those problems are out of the scope of this project. However, the use of biodegradable composites such as wood could be studied and incorporated in future iterations of the project.

8.2.1. Entropy resins & R*Concept

The resin used to manufacture the prototype presents a formulation, denominated Super Sap and produced by **Entropy resins.** As opposed to combinational epoxies, which are mainly petroleum-based, Super Sap epoxy contains bio-renewable materials sourced as co-products or from waste streams of other industrial processes, such as wood pulp and bio-fuels production. These natural components have excellent elongation and exceptionally high adhesion properties. As opposed to 100% petroleum derivated epoxies, the production of Super Sap epoxy supposes a reduction in CO and greenhouse gas emissions of approximately 50%. In addition, it demands less power and water consumption. Furthermore, less harmful by-products are generated.

R*Concept is a company based in Barcelona that specialized in selling bio-resins under its brand. The company is fully compromised with the sustainability of our environment and since 2019 they accomplished the goal of being carbon neutral. This means that all the energy consumed in their facility comes from green sources. If more prototypes had to be made, R*Concept would be the brand of choice.

9. NEXT STEPS

As previously announced, budget and time limitations prevented the manufacturing of a full manufacturing prototype. Therefore, it is a priority to produce a prototype, install it on an Europe dinghy and test the results. Moreover, the studied manufacturing process presents some flaws that need to be rectified. Therefore, it is also fundamental to find solutions to this process or studying new alternatives.

Following this step, the hydrodynamic design could be enhanced by conducting CFD analysis with the appropriate software. In addition, it is primordial to study the drag of the configuration and try to reduce it, a task that could also be done with the CFD software. With the results of the conducted CFD analysis, a structural study of the design could also be performed, followed by a more exhaustive material selection process. The objective is to reduce manufacturing costs and increase the structural safety of the prototype.

On the other hand, the control mechanism needs some refinement and its behaviour has to be mathematically defined to further understand its effects on the ride height. If we remember, it was decided to use a mechanical control mechanism instead of a PID controller. Further analysis of the electrical alternative could be performed since it presents numerous advantages and also it would be a revolutionary concept if successfully installed.

Finally, a marketing study could be done to determine the commercial feasibility of the project. If the results were positive, the prototype would have to be adapted for serial manufacturing through further refinement of the components.

10. CONCLUSIONS

The results of this project demonstrate that old conventional dinghy designs can be adapted to equal the performance of their foiling counterparts. In the case of the Europe dinghy, this is possible by installing two hydrofoils, one in place of the centreboard and the other one instead of the rudder, in a tandem configuration. The result is a compact removable kit that respects the structural integrity of the hull. The design incorporates a control mechanism that adapts the deflection of a flap depending on the ride height, allowing stable flight at speeds nearly twice the one achieved without hydrofoils.

The initial sizing of the foils was done through aerodynamic theory. After intensive research and study of the forces involved during sailing, an algorithm was developed. The outcomes of the approach were then tested using XFLR5 software. The results presented some discrepancies, but by modifying the position of the sailor 10 cm the initial objectives of lift generation and stability were achieved.

After that, a modelling process captured the obtained aerodynamic configuration in a three-dimensional design and the control mechanism was incorporated. All this process was done considering the initial objective of respecting the structural integrity of the dinghy's hull. The design of the control mechanism although successful, its final result was not exhaustively tested and would need some refinement if future work is to be carried out.

The prototype manufacturing process, as well as material selection, was overall the most challenging part of this thesis. Several limitations downgraded the initial objective of manufacturing a fully functional prototype to a sample of the centreboard and flap assembly, to prove that the full manufacturing was possible if more resources were available.

The manufacturing of the flap proved feasible through additive manufacturing and the final results are considered successful. On the other hand, the obtained centreboard prototype which was manufactured using composite materials presented some irregularities which would prevent it from generating the necessary lift. However, the imperfections of the followed process can be easily resolved.

11. BIBLIOGRAPHY

[1] B. Gustav, “Europe dinghy,” [Online]. Available: https://en.wikipedia.org/wiki/Europe_(dinghy)#/media/File:Europe_dinghy.svg. [Accessed 17 March 2021].

[2] Fukillo, “International 14 sailboat plans,” [Online]. Available: http://obosland.blogspot.com/2015/12/buy-international-14-sailboat-plans.html. [Accessed 27 February 2021].

[3] Deecaffari, “Points of Sail,” [Online]. Available: https://www.deecaffari.co.uk/en/did_you_know-edition_07.html. [Accessed 5 March 2021].

[4] TracTrac, “Europe Class YOUTH European Championship 2015,” [Online]. Available: https://tractrac.com/event-page/event_20150703_EuropeClas/537. [Accessed 21 March 2021].

[5] A. J. Acosta, «HYDROFOILS AND HYDROFOIL CRAFT,» 1973.

[6] R. Vellinga, Hydrofoils: design, build, fly, Gig Harbor: Peacock Hill Publishing, 2009.

[7] J. Harding, “America's Cup Class AC75 boat concept revealed,” 21 November 2017. [Online]. Available: https://www.sailing.org/news/85519.php#.YK-JqagzaUk. [Accessed 7 March 2021].

[8] International Moth Class Association, “International Moth Class Association,” [Online]. Available: http://www.moth-sailing.org/get-a-moth/. [Accessed 6 March 2021].

[9] WASZP, “WASZP - The one design foiler,” [Online]. Available: https://www.waszp.com/. [Accessed 13 March 2021].

[10] Merriam-Webster, “Definition of Hydrodynamics by Merriam-Webster,” [Online]. Available: https://www.merriam-webster.com/dictionary/hydrodynamics. [Accessed 2 April 2021].

[11] E. Banihani, “Velocity boundary layer development on a flat plate,” [Online]. Available: https://www.researchgate.net/figure/Velocity-boundary-layer-development-on-a-flat-plate-2_fig1_323218834. [Accessed 7 April 2021].

[12] S. Franchini y Ó. López García, Introducción a la Ingeniería Aeroespacial, Madrid: Instituto Universitario de Microgravedad "Ignacio Da Riva".

[13] S. Pinzón, “Introduction to Vortex Lattice Theory,” 30 September 2015. [Online]. Available: https://publicacionesfac.com/index.php/cienciaypoderaereo/article/view/433/610. [Accessed 15 April 2021].

[14] W. Widodo, “Wingtip vortices cause downwash,” [Online]. Available: https://www.researchgate.net/figure/Wingtip-vortices-cause-downwash-which-reduces-the-effective-angle-of-attack-1_fig1_309476028. [Accessed 6 April 2021].

[15] F. Ohntrup, “Simplified scheme of the mainfoil control system.,” [Online]. Available: https://www.researchgate.net/figure/Simplified-scheme-of-the-mainfoil-control-system_fig2_328571438. [Accessed 15 May 2021].

[16] C. Martin, “Bloomberg Green,” 5 February 2020. [Online]. Available: https://www.bloomberg.com/news/features/2020-02-05/wind-turbine-blades-can-t-be-recycled-so-they-re-piling-up-in-landfills. [Accessed 3 June 2021].

[17] Unknown author, “Carl XCH-4 Hydrofoil,” [Online]. Available: https://en.wikipedia.org/wiki/Hydrofoil#/media/File:Carl_XCH-4.jpg. [Accessed 5 March 2021].

[18] P. B. Serra, «Hydrofoil Design and Construction,» 2019.

[19] S. Karlsson y J. Urde, «Hydrofoiling Europe-Dinghy,» 2018.

[20] J. D. Anderson, Fundamentals of Aerodynamics, Fifth Edition ed., New York: McGraw-Hill Companies, Inc., 2011.

[21] International Europe Class Association (UK), “UK Europe Class Association,” [Online]. Available: https://www.ukeuropeclass.com/. [Accessed 03 March 2021].

[22] Rodacciai, “Normas y tablas,” [Online]. Available: https://www.rodacciai.es/normeetabelle.php?pid=37. [Accessed 2 June 2021].

[23] International Europe Class Union, “International Europe Class Union,” [Online]. Available: http://www.europeclass.org/introduction.html. [Accessed 2 March 2021].

[24] ISAF, “INTERNATIONAL EUROPE CLASS RULES,” 2015.

[25] S & C Thermofluids Ltd, “Coanda Effect,” [Online]. Available: http://www.thermofluids.co.uk/effect.php. [Accessed 19 April 2021].

[26] Factor, «Catálogo General,» 2010.

[27] Bieker Boats, “Bieker Moth | Bieker Boats | Seattle, WA,” [Online]. Available: https://biekerboats.com/project/bieker-moth/. [Accessed 15 March 2021].

[28] SIMPLIFY3D, “Ultimate 3D Printing Materials Guide,” 2021. [Online]. Available: https://www.simplify3d.com/support/materials-guide/. [Accessed 24 March 2021].

[29] CompositesWorld, “Recycling end-of-life composite parts: New methods, markets,” [Online]. Available: https://www.compositesworld.com/articles/recycling-end-of-life-composite-parts-new-methods-markets. [Accessed 5 June 2021].

[30] WWF, “Observatorio de la Electricidad,” 2021.

[31] Oficina Catalana del Canvi Climàtic, “Factor de emisión de la energía eléctrica: el mix eléctrico,” [Online]. Available: https://canviclimatic.gencat.cat/es/actua/factors_demissio_associats_a_lenergia/. [Accessed 3 June 2021].

[32] NASA, “Boundary Layer,” [Online]. Available: https://www.grc.nasa.gov/www/k-12/airplane/boundlay.html. [Accessed 7 April 2021].

[33] Go Sail, “Europe sailing dinghy,” [Online]. Available: https://www.go-sail.co.uk/europe-sailing-dinghy/. [Accessed 16 March 2021].

[34] E. Lazo, “Foil Control Design for Hydrofoil Craft,” 2016. [Online]. Available: https://www.academia.edu/28170875/Masters_Thesis_Foil_Control_Design_for_Hydrofoil_Craft. [Accessed 14 May 2021].

[35] USHA, “Hydrofoiling History - Hydrofoil,” [Online]. Available: http://www.hydrofoil.org/history.html. [Accessed 28 March 2021].


ESP
392